



AALBORG UNIVERSITY
DENMARK

Aalborg Universitet

Glucagon fibrillation - kinetics and structural polymorphism

Andersen, Christian Beyschau

Publication date:
2009

Document Version
Publisher's PDF, also known as Version of record

[Link to publication from Aalborg University](#)

Citation for published version (APA):
Andersen, C. B. (2009). *Glucagon fibrillation - kinetics and structural polymorphism*. Institut for Kemi, Miljø og Bioteknologi, Aalborg Universitet.

General rights

Copyright and moral rights for the publications made accessible in the public portal are retained by the authors and/or other copyright owners and it is a condition of accessing publications that users recognise and abide by the legal requirements associated with these rights.

- Users may download and print one copy of any publication from the public portal for the purpose of private study or research.
- You may not further distribute the material or use it for any profit-making activity or commercial gain
- You may freely distribute the URL identifying the publication in the public portal -

Take down policy

If you believe that this document breaches copyright please contact us at vbn@aub.aau.dk providing details, and we will remove access to the work immediately and investigate your claim.

Glucagon fibrillation — kinetics and structural polymorphism

Christian Beyschau Andersen

Ph.D. Thesis

Protein Structure and Biophysics, Novo Nordisk A/S

&

Department of Life Sciences, Aalborg University

Ph.D. thesis

Ph.D. thesis by Christian Beyschau Andersen under the Industrial PhD programme. Supervised by Christian Rischel (Novo Nordisk) and Daniel Erik Otzen (now Aarhus University). Thesis work initiated December 1st, 2004.

Contacts:

C.B.A.^{1,2} +45 44 42 62 66, cbya@novonordisk.com

D.E.O.³ +45 20 72 52 38, dao@inano.dk

C.R.¹ +45 44 42 05 13, cris@novonordisk.com

¹ Novo Nordisk A/S, Protein Structure and Biophysics, Novo Nordisk Park, DK-2760 Måløv.

² Aalborg University, Department of Life Sciences, Sohngaardsholmsvej 49, DK-9000 Aalborg.

³ Aarhus University, Interdisciplinary Nanoscience Centre, Gustav Wieds Vej 10 C, DK-8000 Århus C.

© Christian Beyschau Andersen, 2008

Ph.D. thesis

1st Ed., 10 copies.

Novo Nordisk A/S

Novo Nordisk Park

DK-2760 Måløv

Denmark

Table of contents

Glucagon fibrillation — kinetics and structural polymorphism.....	ii
Ph.D. thesis.....	iv
Table of contents.....	v
Preface and acknowledgments.....	vii
Resumé (Danish summary).....	ix
Summary.....	xi
Abbreviations.....	xiii
Papers.....	xiv
Papers included in the thesis.....	xiv
Papers not included in the thesis.....	xiv
1. Introduction.....	2
1.1 Historical preamble.....	2
1.2 Amyloid diseases.....	2
1.3 Glucagon.....	3
1.4 Subject of the thesis.....	5
1.4.1 The molecular basis for glucagon's structural polymorphism.....	5
1.4.2 Morphology selection via morphology-dependent growth inhibition.....	5
1.4.3 Glucagon fibrils multiply by branching.....	6
2. Fibril structure and polymorphism.....	8
2.1 Folding and misfolding of proteins.....	8
2.2 Amino acid properties affect fibrillation.....	10
2.3 Prediction of fibril propensity.....	11
2.4 Fibrils are built from protofilaments.....	15
2.5 Fibril structure at atomic resolution.....	17
2.6 Fibril criteria.....	19
2.6.1 Transmission electron microscopy.....	20
2.6.2 Fiber diffraction.....	21
2.6.3 Fibril-specific fluorescent dyes.....	22
2.7 Intrinsic Trp fluorescence.....	23
2.8 Linear dichroism.....	25
2.9 Proteolysis of fibrils.....	26
3. Selection of morphologies.....	30
3.1 Templated fibril growth.....	30

3.2	Morphology-dependent growth inhibition	33
4.	Fibrillation kinetics.....	38
4.1	Nucleation-dependent aggregation.....	38
4.2	Oligomeric species and protofibrils	39
4.3	Secondary nucleation mechanisms	41
4.4	Glucagon fibril branching in surface layers	43
4.5	TEM pictures of branching glucagon fibrils.....	47
4.6	Kinetics in bulk solution.....	48
4.7	Criteria for the existence of secondary nucleation mechanisms.....	50
5.	Prion diseases	54
5.1	Strain encoding.....	55
5.2	Transmissibility.....	55
5.3	Strain stability	57
6.	Specialized techniques	60
6.1	Total internal reflection fluorescence microscopy	60
6.2	Fiber diffraction.....	62
6.3	Small-angle light scattering	64
7.	Conclusion	66
8.	Papers.....	68
8.1	Glucagon amyloid-like fibril morphology is selected via morphology-dependent growth inhibition.....	68
8.2	Branching in amyloid fibril growth	68
9.	References.....	70

Preface and acknowledgments

This thesis highlights the work done from December 1st, 2004 to Januar 31st, 2008 by undersigned in order to obtain the Ph.D. degree. The work was done under the Industrial PhD programme financed by Ministry of Science, Technology and Innovation and Novo Nordisk A/S and to that end an Industrial PhD report has been submitted and approved separately.

I am very grateful to my supervisors Christian Rischel and Daniel Otzen for the dedicated supervision and commitment, I have received for the past three years. The main part of the work was carried out at Department of Protein Structure and Biophysics, Novo Nordisk, and I greatly appreciate the many friendly colleagues found in this and neighbouring departments. You are all acknowledged for generously taking your time to patiently teach me new techniques and discuss data. Mathias Norrman, Anders Svensson, Gerd Schluckebier have collected X-ray data in-house as well as at Maxlab, Sweden. Simon Bjerregaard and Henning Thøgersen contributed with insights into the fibrillation propensity of glucagon and related peptides. Brian Vandahl and Henrik Rahbek-Nielsen introduced me to MS and patiently helped me identify the digest fragments. Finally, Novo Nordisk and Ministry of Science, Technology and Innovation have co-financed the project and Christian Rischel and Head of Department, Hanne B. Rasmussen, are gratefully acknowledged for help finding funding for the Ph.D. project as well as funding for the postdoc at CNR in Palermo, which I will start February 1st 2008. Thank you!

Parts of the project took place at Department of Life Sciences, Aalborg University, and each time I have been warmly welcomed by the group of Daniel Otzen. The Ph.D. project is based on the tremendous amount of work performed by Ph.D. Jesper Søndergaard Pedersen, with whom I truly appreciate the friendship as well as hours of scientific discussions. Professor Gunna Christiansen has several times assisted with electron microscopy images and always with great enthusiasm.

My supervisors missed no chance to send me abroad to visit colleagues in exotic parts of the world. The opportunities seized during these visits have multiplied throughout my Ph.D. Dr. Goto warmly welcomed me to his lab in fall 2006. The three months I spent there were culturally and scientifically among the greatest experiences of my life. The Osakan generosity and curiosity—especially that of Dr. Hisashi Yagi, Dr. Masanori Yagi, Dr. Tadato Ban, and Dr. Yuji Goto—will not be forgotten. The visit in Osaka will stay with me for the rest of my life thanks to you. Louise Serpell at University of Sussex introduced me to the art of fiber diffraction in what must

have been the hottest summer in Brighton ever. I sincerely appreciate the substantial amount of help I received during and after the visit. Enzo, Mauro and Rita twice welcomed me to CNR, Palermo, apparently a place I cannot seem to let go off. Thank you for introducing me to light scattering as well as Sicilian hospitality. I am truly looking forward to continuing working with you for the next two years.

Last but not least, family and friends are acknowledged for most appreciated non-scientific discussions. Thanks!

Måløv, January 31st, 2008

Christian Beyschau Andersen

Resumé (Danish summary)

Emnet for denne ph.d. afhandling er fibrillering af glucagon. Glucagon er et naturligt forekommende hormon bestående af 29 aminosyrer, som sammen med insulin kontrollerer blodsukkeret i mennesker. Ved frigivelse fra pancreas øger glucagon blodsukkeret, mens insulin har den stik modsatte effekt. Glucagon sælges af Novo Nordisk til behandling af akut hypoglukæmi. Som en lang række andre peptider og proteiner har glucagon en naturlig tendens til at danne lange uopløselige proteinstrukturer kaldet fibriller. Fibrillering kan bl.a. være et problem under produktion af biofarmaceutika (proteinbaserede lægemidler) og ved henstand i flydende formulering. En anden interesse i fibrillering stammer fra en lang række uhelbredelige og fatale sygdomme, som alle tilskrives fibrillering af et specifikt protein i en specifik vævstype. Som eksempel, menes Alzheimers at skyldes dannelsen af fibriller eller fibrilrelaterede strukturer af amyloidd β -peptid i hjernen.

Et interessant kendetegn ved fibrilstrukturer observeret med elektronmikroskopi er deres polymorfi. Glucagonfibriller er ingen undtagelse, idet de ved lav peptidkoncentration (0.25 mg/mL) består af to eller flere protofilamenter, der snor sig repetitivt om hinanden, mens de ved høj koncentration (8 mg/mL) består af et enkelt usnoet protofilament. Det er i det store hele uvist, hvorfra fibrillers polymorfi stammer: Skyldes det polymorfi af protofilamenterne, der danner de modne fibriller, eller repræsenterer polymorfi forskellige måder at kombinere identiske protofilamenter lateralt? Det er bemærkelsesværdigt, at glucagon fibrillers morfologi kan udvælges ved at ændre blot én parameter, peptidkoncentrationen. Denne egenskab gør det nemlig muligt at undersøge mekanismen bag udvælgelsen af fibrilmorfologier. Samtidig er det muligt at karakterisere den snoede og den lige morfologiske strukturelle egenskaber. Polymorfi er gennem de senere år blevet vist at være vigtig i forståelsen af visse prionsygdommes evne til at transmittere fra individ til individ, sommetider på tværs af artsbarrierer.

Selve dannelsen af fibriller fra en proteinopløsning udviser ofte et sigmoidt forløb, karakteriseret ved en lang lagfase, hvor der ikke sker betydelig tilvækst af fibrilmasse, efterfulgt af en fase hvor fibrilmassen stiger drastisk. Denne reaktionsprofil kan ikke alene forklares ved en simpel nukleeringsproces efterfulgt af vækst fra fibrilenderne. En mulig forklaring er, at der findes en sekundær nukleeringsmekanisme, som kontinuerligt danner nye fibrilender proportionalt med den allerede dannede fibrilmasse. Denne forklaring lider dog under en udtalt mangel på ekspe-

rimentelle beviser for, at en sådan nukleeringsmekanisme overhovedet eksisterer. Glucagon har også en sigmoid reaktionsprofil og vba. specialiserede biofysiske teknikker blev baggrunden for dette fibrilleringsforløb studeret. Sekundære nukleeringsmekanismers vigtighed understreges af deres indflydelse på prionstammers fænotype og stabilitet.

I dette ph.d. arbejde er benyttet en række biofysiske teknikker, både traditionelle teknikker så som cirkulær dikroisme, dynamisk lysspredning, fluorescensspektroskopi og elektronmikroskopi, men også en række mere specialiserede teknikker: Småvinkellysspredning, total intern reflektionsfluorescensmikroskopi (TIRFM) samt fiberdiffraktion. Disse er tilegnet ved ophold hos forskningsgrupper i Palermo, Osaka og Brighton.

Ph.d. arbejdets tre hovedresultater er:

1. Glucagon fibriller dannet ved 0.25 mg/mL glucagon er snoede, mens de ved 8 mg/mL er lige. Der er en strukturel forskel på de to morfologier bestemt ved forskelle i bl.a. fiberdiffraktionsmønstre, lineær dikroismespektre samt proteolytisk fordøjelse. Dette antyder, at de to morfologier er dannet af strukturelt forskellige protofilamenter.
2. Skiftet i morfologi fra snoet til lige sker gradvist og korrelerer med dannelsen af reversible trimerer. Krydsseedingsforsøg afslører, at seeds af lige morfologi har en udtalt virkning på fibrilleringskinetikken ved 0.25 mg/mL, hvorimod seeds af snoet morfologi ingen effekt har på fibrilleringskinetikken ved 8 mg/mL glucagon. Vi konkluderer, at reversibel hæmning af snoede fibriller med glucagon trimerer er årsagen til udvælgelsen af den lige fibrilmorfologi ved høj koncentration.
3. Glucagons fibrilleringskinetik har et sigmoidt forløb, som antyder at fibrilmassen vokser proportionalt med den på et givent tidspunkt dannede fibrilmasse. Med TIRFM og småvinkellysspredning på seedede opløsninger af glucagon blev det vist, at glucagonfibriller er i stand til at forgrene sig kontinuerligt både på quartz overflader og i opløsning. Baseret på seedet fibrilleringskinetik blev et kriterium for eksistensen af sekundære processer opstillet: I deres fravær påvirkes udelukkende fibrilmassens vækstrate, mens deres tilstedeværelse udelukkende påvirker lagfasen. Ved sammenligning med A β (1-40), et peptid som tidligere er vist at danne uforgrenede fibriller, blev kriteriet valideret.

Summary

The subject of this Ph.D. thesis is fibrillation of glucagon. Glucagon is a naturally occurring hormone consisting of 29 amino acids, which together with insulin regulate the blood sugar in humans. When released from the pancreas, glucagon increases the blood sugar, while insulin has the exact opposite effect. Glucagon is marketed by Novo Nordisk as a drug to treat severe hypoglycaemia. As most peptides and proteins, glucagon has an inherent propensity to form long insoluble protein structures, fibrils. Fibrillation is often a problem during the production of biopharmaceuticals (drugs based on proteins) and when formulating proteins. Another interest in fibrillation is due to a large number of incurable and fatale diseases assumed to be caused by fibrillation of a specific protein in a specific location. As an example, Alzheimer's disease seems to evolve from the formation of fibrils or fibril-related structures of amyloid β -peptide in the human brain.

An interesting feature of fibril structures observed by electron microscopy is their polymorphism. Glucagon fibrils are no exception as they at low peptide concentration (0.25 mg/mL) consist of two or several repetitively twisting protofilaments, while they at high concentration (8 mg/mL) consist of a single nontwisting protofilament. The origin of fibril polymorphism is largely unknown: is it caused by polymorphism of the protofilaments forming the mature fibrils, or do polymorphism represent different ways to organize otherwise identical protofilaments? Surprisingly, by changing just one parameter, the glucagon concentration, it is possible to select a specific morphology. This property enables studying the mechanism behind the selection of morphologies, and at the same time, it enables characterizing the structural properties of the twisted and straight morphology. Recently, polymorphism has been shown to be important for the understanding of the ability of prion diseases to transmit between individuals, sometimes crossing the species-barrier.

The formation of fibrils in a protein solution often exhibit a sigmoid reaction profile, characterized by a long lag phase, in which minute amounts of fibril mass are formed, followed by a phase of rapid fibril growth. This reaction profile cannot be explained by a simple nucleation process followed by growth from the fibril ends. A possible explanation suggests the existence of a secondary nucleation mechanism, which continuously generate new fibril ends in proportion to the already formed fibril mass. This explanation does, however, suffer from a pronounced lack of ex-

perimental evidence that such a mechanism should even exist. Glucagon has also a sigmoid reaction profile, and using specialized biophysical techniques the origin of the kinetics was studied. The importance of secondary nucleation mechanisms is stressed by their influence on the phenotype and stability of prion strains.

In this Ph.D. work a number of biophysical techniques have been applied, including traditional techniques such as circular dichroism, dynamic light scattering, fluorescence spectroscopy, and electron microscopy; but also a number of specialized techniques: small-angle light scattering, total internal reflection fluorescence microscopy (TIRFM), and fiber diffraction. These techniques have been obtained through visits at research groups in Palermo, Osaka, and Brighton.

The three main results of the Ph.D. work are:

1. Glucagon fibrils formed at 0.25 mg/mL are twisted, while at 8 mg/mL they are straight. Structural differences between the two morphologies manifest themselves in, *e.g.*, fiber diffraction patterns, linear dichroism spectra, and proteolytic digest. The results suggest that the two morphologies are formed from structurally different protofilaments.
2. The change in morphology from twisted to straight occurs gradually when the peptide concentration is increased and correlates with the formation of reversible trimers. Cross-seeding experiments reveal that seeds of straight morphology have a pronounced effect on the fibrillation kinetics at 0.25 mg/mL, while seeds of twisted morphology no effect have on the fibrillation kinetics at 8 mg/mL glucagon. We conclude that reversible inhibition of twisted fibrils by glucagon trimers is the reason for the selection of the straight morphology at high concentration.
3. Glucagon's fibrillation kinetics have a sigmoid profile, which indicates that the fibril mass grows in proportion to the fibril mass present at any given time. Using TIRFM and small-angle light scattering on seeded solutions of glucagon, it was shown that glucagon fibrils continuously create new fibril ends by branching. Based on seeded fibrillation kinetics, a criterion for the existence of secondary processes was proposed: in their absence, only the fibril mass growth rate is affected, while their presence only affects the lag phase. By comparison with A β (1-40), a peptide previously shown to form unbranched fibrils under physiological conditions, the validity of the criterion was confirmed.

Abbreviations

AFM	Atomic force microscopy
A β (1-40)	Amyloid β -peptide residue 1-40
BSE	Bovine spongiform encephalopathy
CD	Circular dichroism
CJD	Creutzfeldt-Jakob's disease
EM	Electron microscopy
GLP-1	Glucagon-like peptide 1
GLP-2	Glucagon-like peptide 2
LALS	Large-angle light scattering
LD	Linear dichroism
PrP	Prion protein
SALS	Small-angle light scattering
ssNMR	Solid state nuclear magnetic resonance
TEM	Transmission electron microscopy
ThT	Thioflavin T
TIRFM	Total internal reflection fluorescence microscopy
vCJD	Variant Creutzfeldt-Jakob's disease
β_2 M	β_2 -microglobulin

Amino acids are abbreviated using the one- and three letter symbols suggested by IUPAC.

Papers

Papers included in the thesis

Andersen, C. B., Otzen, D., Christiansen, G., and Rischel, C. *Glucagon Amyloid-like Fibril Morphology Is Selected via Morphology-Dependent Growth Inhibition* *Biochemistry* (2007) **46**, 7314-7324.

Andersen C. B., Yagi H., Manno M., Martorana V., Christiansen G., Otzen D. E., Goto Y., Rischel C. *Branching in amyloid fibril growth* **submitted**.

Papers not included in the thesis

Andersen C. B., Serpell L. C., Hicks M., Svensson M., Norrman M., Rahbek-Nielsen H., Vandahl B., Christiansen G., Rischel C., Otzen D. E. *The molecular basis for glucagon's structural polymorphism* **manuscript in preparation**.

Nesgaard, L. W., Hoffmann, S. V., Andersen, C. B., Malmendal, A., Otzen, D. E. *Characterization of Dry Globular Proteins and Proteins Fibrils by Synchrotron Radiation Circular Dichroism* **submitted**.

Holm N. K., Jespersen S. K., Thomassen L. V., Wolff T. Y., Sehgal P., Thomsen L. A., Christiansen G., Andersen C. B., Knudsen A.D., Otzen, D. E. *Aggregation and fibrillation of bovine serum albumin* *Biochimica et Biophysica Acta* (2007) **1774**, 1128-1138.

1. Introduction

In this chapter, an introduction to the field of fibrillation is presented from the first accounts of fibrils in human tissue to the challenges faced today when formulating future protein-based pharmaceuticals. The short historical introduction is followed by an introduction to the model peptide, glucagon, studied during this Ph.D. project. Toward the end of the chapter, the subject of the thesis is detailed.

1.1 *Historical preamble*

In 1639, Nicolaus Fontanus reported what is believed to be the first account of amyloidosis. In an autopsy of a young man, he discovered that the deceased had a large spleen filled with white stones. Later medical accounts found similar deposits of what appeared to be fat or starch in various organs including liver, kidneys, and brain. In 1854, Rudolph Virchow used the term amyloid (from Latin, *amylum*, starch) to describe the deposits, as he had noticed, they stained blue with iodine. In some cases, as for example systemic amyloidosis, several kilograms of proteins could be deposited (1). Five years later, in 1859, Carl Friedreich and August Kekulé reported that the spleen deposits were chemically identical to albumin, and hence of proteinaceous nature (2). It was not until 1959, Cohen and Calkins recognized that when examined by electron microscopy (EM), all types of amyloid deposits—whether formed *in vivo* or *in vitro*—consisted of non-branching fibril structures (3). Even today, the term amyloid is used in connection with fibrils as a reminder of the highly ordered structure fibrils share with starch. Amyloid fibrils have since their discovery been considered misfolded structures serving no functional purposes to the organism. This understanding has been challenged in recent years with the discovery of certain functional amyloids as reviewed by Otzen and Nielsen (2007) (4). Functional amyloids include components in spider's web (spidroins) and adhesion fibrils on the surface of bacteria (CsgA).

1.2 *Amyloid diseases*

The human body contains an estimated 25 000 genes each encoding up to several different proteins and peptides (5). Each protein is formed from a string of amino acids, which fold into a specific three-dimensional structure from which the protein exerts its function. Failure to attain the structure can potentially harm the human organism, and to that end a number of cellular security measures have evolved that detect and degrade misfolded proteins. In a number of cases, these quality control

systems fail, and as a result misfolded proteins accumulate (6). Often these plaques of aggregated proteins manifest themselves as severe diseases. A special class of highly ordered aggregates, fibrils, have gained special interest due to their severity. In humans, more than 40 diseases related to fibrils are known (7, 8). Each disease is linked to the fibrillation of a specific protein in a specific location (Section 4.2). As an example, fibrillation of amyloid β -peptide ($A\beta$) in the brain is closely linked to Alzheimer's disease. Amyloid diseases such as Parkinson's disease and Alzheimer's disease rank among the most enervating, socially disruptive not to mention costly diseases of the modern world (9). As of today, no treatment exists for amyloid diseases, but the first Alzheimer's disease drug candidates, which all aim at reducing the amount of protofibrillar $A\beta$ aggregates, are now being tested in the clinic (10). A disease caused by fibrillation of a given protein often show variations in terms of phenotypes and incubation periods. This phenomenon is referred to as strains and is thought to be connected to the fact that fibrils can have various structural isoforms known as morphologies (11).

1.3 Glucagon

Glucagon is a peptide hormone derived from the proglucagon precursor, which in the α -cells of the pancreatic islets of Langerhans is processed to glucagon and a larger fragment, designated 'major proglucagon fragment' (12). In the gut endocrine cells, proglucagon is processed to the glucagon-like peptides GLP-1 and GLP-2, which are involved in the intake, absorption, retention and disposal of energy. More specifically, GLP-1 stimulates insulin and inhibits glucagon secretion from the islet β and α cells, respectively, in a glucose-dependent manner. Hence, once plasma glucose returns to normal, GLP-1 no longer stimulates insulin or inhibits glucagon secretion. Proglucagon contains three other peptides, shown schematically in Figure 1, which also share sequence-similarity with glucagon.

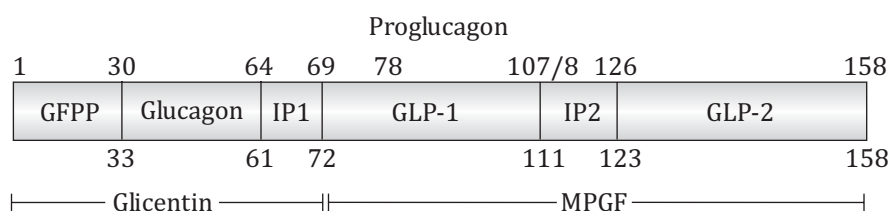


Figure 1. Proglucagon contains a number of peptides with similar primary structures. Glucagon and GLP-1 are involved in the regulation of blood sugar levels and the function of GRPP, IP1, IP2, and GLP-2—although not understood in detail—is related to the development and regulation of the gastric organs. Adapted from reference (12).

Glucagon itself generally functions as a counter-regulatory hormone, opposing the actions of insulin, and maintaining the levels of blood glucose. The hormone has 29 residues and a molecular weight of 3 843 Da. In peripheral tissue and especially the liver, the insulin-to-glucagon ratio controls the release and uptake of plasma glucose, which in the human body is kept between 4–8 mmol under normal conditions. Failure to keep this level leads to either hypoglycaemia (low blood sugar) or hyperglycaemia (high blood sugar). In severe cases, hypoglycaemia can lead to coma and—if untreated—even brain damage or death. In diabetics, the counter-regulatory responses to hypoglycaemia are frequently impaired, a defect most often associated with reduced or absent glucagon responses. This is a critical issue, as current diabetes treatment with intensive insulin administration usually increases the risk and frequency of hypoglycaemic events. Although the mechanisms regulating the sensing and response to hypoglycaemia are not fully understood, glucose sensors in the brain (hypothalamus and brainstem) and portal system play important roles in this counter-regulatory system (13).

Glucagon is manufactured by Novo Nordisk as a drug against severe hypoglycaemia. Formulated at pH 2.5, glucagon readily forms fibrils, and this property renders manufacturing of glucagon difficult. At the same time, fibrillation is a key reason why a liquid formulation has not been achieved. Knowledge of the glucagon fibrillation process could very well facilitate production and possibly render a liquid formulation possible. Another interest in the fibrillation properties of glucagon comes from the sequence similarity to GLP-1 (14). GLP-1 analogues are currently in

development as new drugs against diabetes (12, 15). The high sequence similarity between glucagon and GLP-1 makes it likely that new knowledge about glucagon fibrillation can be applied to future liquid formulations of GLP-1. So far, possibly due to the competitive situation surrounding GLP-1 analogues, only few GLP-1 fibrillation studies have been published (16). Last but not least, independently of their proteinaceous origin, all fibrils share a common fibril forming mechanism and structure, and glucagon can thus be used as a model system to elucidate general properties of fibrils.

1.4 Subject of the thesis

The subject of this thesis work is related to the structural polymorphism of glucagon fibrils and the kinetics of glucagon fibrillation and falls in three parts. Common to each of the three sub-projects is that they involved collaboration with external partners in Denmark and abroad.

1.4.1 The molecular basis for glucagon's structural polymorphism

Independently of the protein and the experimental conditions, fibrillated samples consist of a plethora of morphologies when examined by transmission electron microscopy (TEM). This is also the case for glucagon (17). Apparently, for glucagon, a strong dependence of morphology relates to the peptide concentration alone: a twisted morphology is formed at 0.25 mg/mL and a straight morphology is formed at 8 mg/mL. Thus by carefully selecting growth conditions, it becomes possible to guide the glucagon fibrils toward a specific morphology. Whether morphologies represent distinct structural entities or rather represent different ways of assembling otherwise identical protofilaments is still debatable (18). The project aimed at giving new insight to this question by characterizing the two morphologies in terms of structural biophysical properties.

The work included fiber diffraction experiments in the lab of Dr. Louise Serpell, Department of Biochemistry, University of Sussex. A manuscript, *The molecular basis for glucagon's structural polymorphism*, is currently in writing.

1.4.2 Morphology selection via morphology-dependent growth inhibition

The question as to why one morphology is more prevalent under one set of conditions than under another is poorly understood. Glucagon fibrils offer a unique possibility to shed light on this question as their morphology shifts by changing only

one parameter: the peptide concentration. As mentioned above, at 0.25 mg/mL the fibril morphology is twisted, and at 8 mg/mL it is straight. In an interval between these two concentrations, a mixture of both morphologies is present. By combining cross-seeding experiments with insight into glucagon's ability to self-associate, a new understanding of fibril morphology selection emerged.

The work included TEM experiments in collaboration with Dr. Gunna Christiansen, Institute of Medical Microbiology and Immunology, University of Aarhus, and an article, *Glucagon amyloid-like fibril morphology is selected via morphology-dependent growth inhibition*, was published in *Biochemistry* (19).

1.4.3 Glucagon fibrils multiply by branching

Glucagon fibrillation kinetics are characterized by a sigmoid reaction profile with a growth phase significantly shorter than the preceding lag phase (20-23). The abruptness of the transition cannot be explained by spontaneous (fiber-independent) nucleation alone; instead the exponential nature of the reaction profile suggests that a secondary (fibril-dependent) nucleation pathway is involved. Real-time total internal reflection fluorescence microscopy (TIRFM) observations of seeded glucagon solutions showed single-fibrils growing along the quartz surface by addition of monomers to seed ends and continuous branching from fibrils already formed. Light scattering experiments performed under similar conditions demonstrated an abrupt increase in fibril mass suggesting that branching is not restricted to the surface-layer, but also plays an important role in bulk solution kinetics. Based on seeded solutions, a new method to distinguish processes with a secondary nucleation mechanism from processes without such a mechanism was introduced: in the absence of a secondary nucleation mechanism, the effect of increasing the seed concentration is to increase the mass growth rate, while in its presence increasing the seed concentration decreases the lag phase but conserves the exponential nature of the growth.

TIRFM experiments were performed in collaboration with the group of Dr. Yuji Goto, Institute for Protein Research, Osaka University. In addition, light scattering experiments were done in collaboration with Dr. Vincenzo Martorana and Dr. Mauro Manno, Institute of Biophysics, Consiglio Nazionale delle Ricerche, Palermo. A manuscript, *Branching in amyloid fibril growth*, has been submitted for publication.

2. Fibril structure and polymorphism

In this chapter, the structural properties of fibrils are detailed along with some of the basic biophysical techniques used in the characterization of fibrils exemplified by work done on glucagon fibrils during the Ph.D. project. An interesting aspect of glucagon fibrils is their inherent polymorphic properties. Not only does glucagon form a variety of morphologies easily distinguishable by TEM, but by changing the peptide concentration alone, it is possible to select a specific morphology. This provides an excellent platform for studying the structural differences and the mechanism behind the selection of morphologies.

2.1 Folding and misfolding of proteins

The central dogma of molecular biology is that the genetic code stored in DNA is transcribed to RNA, and RNA is translated into a string of amino acids (24). The amino acid chain spontaneously folds into a specific three-dimensional structure, the protein. At least for smaller proteins, the folding process is governed exclusively by the properties of the amino acid residues as demonstrated by Anfinsen's work on ribonuclease in the late 1950's to early 60's (25). Considering the number of amino acids in a typical globular protein and the high degree of conformational freedom in the polypeptide chain, the Anfinsen hypothesis apparently leads to a paradox as originally stated by Levinthal (26). Levinthal concluded that in order to reach the most stable configuration, the protein cannot simply do a random conformational search. In fact, the new view that emerged in the following years involved the concept of an energy landscape for each protein describing the free energy of the polypeptide chain as a function of its conformation (27). As the native state is approached, the conformational degrees of freedom is reduced and the energy landscape is hence likened to a funnel (28). Experiments suggest that the underlying mechanism can be described as nucleation-condensation, in which a small number of key residues form a folding nucleus to which the remainder of the structure condenses (29). For larger proteins, several folding nuclei domains may exist, and these proteins generally fold independently in different domains, which then in a final step are locked into the final structure.

Misfolding, with fibrillation representing a prominent example, is due to exposure of regions of the protein that are normally buried. The cell has many mechanisms, including chaperones, to avoid this, but in some cases, misfolded proteins escape the protective mechanisms of the cell and accumulate within cells or in the

extracellular space. In contrast to protein folding, the formation of fibril structures is mostly a property of the protein backbone, and in general, there is no overlap between the folding nucleus regions and the amino acids prone to fibrillation (30). As the protein backbone is common to all proteins, independently of the amino acid residues, the fibril structure is now considered a general feature of all proteins, including proteins not associated with any disease (27, 31).

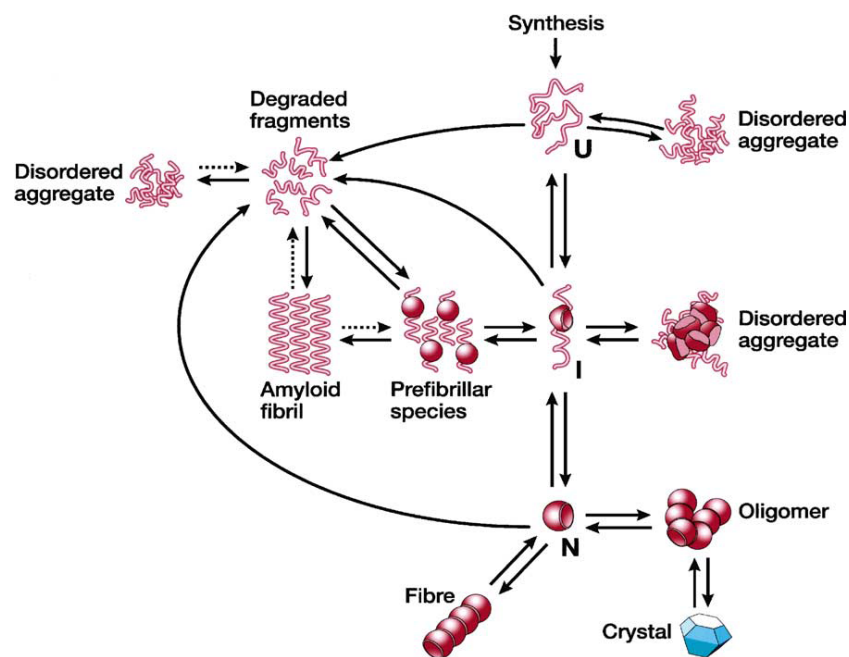


Figure 2. Folding pathways highlighting the faith of a newly synthesized polypeptide chain. Reprinted from reference (30).

Figure 2 recapitulates the possible structural fates of a newly synthesized polypeptide chain. Initially a folding nucleus is formed, which guides the rest of the chain into the state of lowest energy, the native state. The native state may form reversible oligomers (dimers and hexamers in the case of insulin) or fibers (*e.g.*, actin and myosin). The unfolded and partly unfolded state may end up in stable misfolded states and form disordered aggregates. This process is often reversible through the action of chaperones. Fragments of the original polypeptide may be formed by the cellular quality control system, and these fragments may be converted to fibrils as is the case of A β (32). As is shown in the figure, fibrils represent highly stable and insoluble aggregates from which the monomeric polypeptide is not easily recovered.

2.2 Amino acid properties affect fibrillation

Although the fibril backbone structure is basically connected through hydrogen bonding of the protein backbones, there is an effect of the individual residues on the fibril stability and fibrillation propensity. Hydrophobic and aromatic residues, such as Trp, Phe, Tyr, Ile, and Val, are highly prone to fibrillate and long consecutive stretches of such amino acids are selected against in nature (33). In contrast, charged residues, like Lys, Glu, and Arg, help keeping proteins in solution and hence decrease the propensity to fibrillate. In fact, to avoid fibrillation these charged residues are often found on either side of segments containing residues prone to aggregation (33). Pro and Gly are of special interest. The Pro residue has special structural constraints that make it difficult for it to form a β -sheet structure. For this reason, Pro has been termed ' β -breaker' or 'gatekeeper residue' (34, 35). Gly is the smallest amino acid with a single hydrogen atom as its residue. Owing to this, Gly is highly flexible, and incorporation of Gly in a secondary structure element comes at a high entropic cost (8, 36). In the light of these amino acid properties, the strategy for a peptide—such as glucagon—that wishes to remain intrinsically disordered should be clear: avoid the hydrophobic residues, strive for a high net charge, and add a few Pro residues. Curiously, referring to the amino acid sequence of glucagon in Figure 3, glucagon does not seem to follow this strategy.

HSQGTFTSDY SKYLD SRR AQ DFVQWLMNT

Figure 3. The amino acid sequence of glucagon, containing 29 residues. Glucagon has five aromatic residues (blue), five hydrophobic residues (pink), and six charged residues (green). Amino acid properties were assigned using GPMaw (37).

The peptide has five aromatic residues (blue) and additionally five hydrophobic residues (pink). It has six charged residues (green), three positively charged and three negatively charged, and an isoelectric point at $pI = 7.7$. This implies that the peptide solubility at physiological pH is very low. Reasons why glucagon still avoids aggregation *in vivo* include the fact that the glucagon plasma concentration is in the nanomolar range and that the plasma half life is in the order of a few minutes (38-40).

2.3 Prediction of fibril propensity

A number of algorithms have been developed in order to predict the regions prone to fibrillation (33, 41, 42). One such algorithm is TANGO developed by the group of Luis Serrano (2004) (41). TANGO incorporates five different conformational states of the protein— β -turn, α -helix, β -sheet, the folded state, and β -aggregates—and different energy terms, taking into account hydrophobicity and solvation energies, electrostatic interactions and hydrogen bonding. For each residue in a peptide, TANGO computes the percent occupancy of the β -aggregation conformation. Five consecutive residues with a score higher than 5 % pr. residue were classified as having some aggregation tendency. TANGO was previously applied to glucagon by Pedersen *et al.* in a study, which predicted residues 22-27 (FVQWLM) to have a score higher than 5 % (43). This stretch contains two aromatic residues (F and W) and three hydrophobic residues (V, L, and M). The remainder of the glucagon structure was assigned scores equal to or close to zero. The TANGO plot is shown in Figure 4.

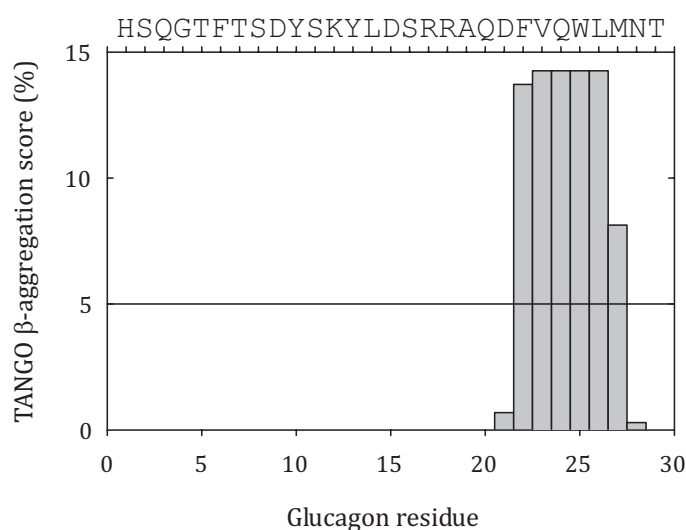


Figure 4. TANGO algorithm applied to glucagon under the conditions used in this thesis. Glucagon, with six consecutive residues with a β -aggregation score higher than 5 %, has some aggregation tendency according to TANGO. The calculation was performed using the web-based TANGO-interface (44).

In a comparison with aggregation studies of 179 peptide sequences found in the literature, TANGO was found to be highly accurate as only 9 out of 62 predictions

were false positives. In general, a guideline of 5 consecutive residues having a β -aggregation score higher than 5 % turned out to be a good predictor of aggregation propensity independently of the size of the peptide or protein. Furthermore, the group measured a set of 71 peptides to test if the false predictions are due to experimental error in the dataset or due to inaccuracies in the algorithm, and found a slightly lower correlation compared to the literature-derived set (41).

We have applied a more recent algorithm, PASTA, to the glucagon sequence (42). PASTA is a computational approach based on the propensities of two residues to be facing each other on neighbouring strands in a β -sheet. Hence, the basic assumption is that the same interactions found in structures of known globular proteins are also found in the fibril backbone. The method assigns energy scores to fragments of the same length from the peptide in both parallel and antiparallel orientations. Compared to other algorithms, PASTA is able to predict the registry of the intermolecular hydrogen bonds between fibril-prone sequences, and PASTA is able to discriminate between parallel and antiparallel β -strand configurations. The ability of the algorithm to correctly predict aggregation prone regions was tested on three designed polypeptides, whose structure is known from X-ray diffraction and ssNMR, and on five well-characterized, natively unfolded proteins, including A β (1-40) (42). For the natively unfolded proteins, PASTA generally correctly predicted the observed tendency of specific amino acid stretches to assemble into parallel β -sheets. The algorithm was also able to correctly determine the parallel or antiparallel orientation of β -strands as confirmed by applying PASTA to short designed polypeptides, whose structure had been determined experimentally. Later, the algorithm was tested on a set of natively folded proteins and once again the ability of the algorithm to predict regions prone to aggregation was very high (45).

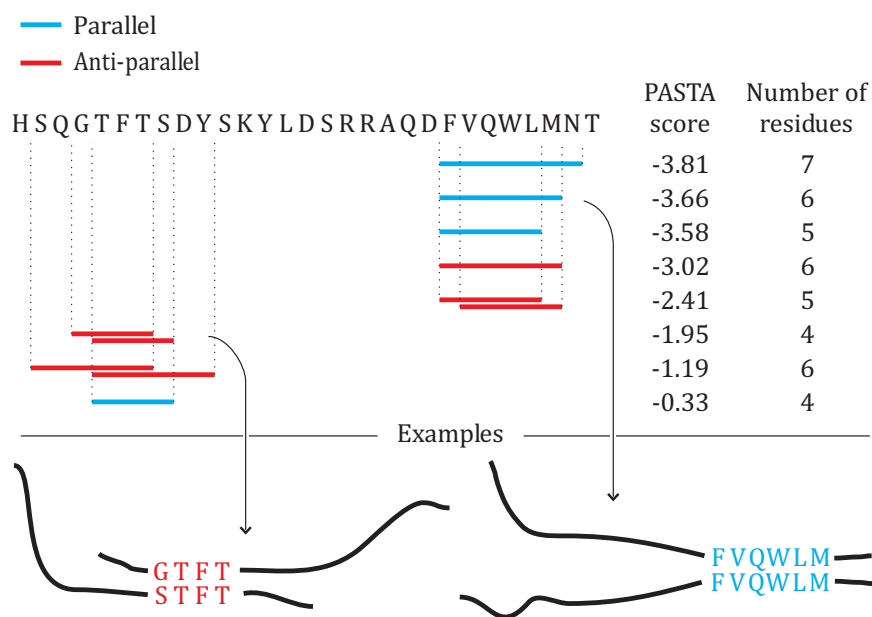


Figure 5. Fibrillation-prone regions of glucagon as predicted by PASTA. Blue lines indicate parallel configuration and red lines indicate antiparallel configurations as exemplified in the bottom part of the figure. A single line indicates in-register configurations. PASTA calculation by Henning Thøgersen, Novo Nordisk.

In Figure 5, the fibril-prone areas of glucagon as predicted by PASTA are shown and the parallel/antiparallel configurations exemplified. In comparison with the TANGO algorithm, which only predicts the region containing residues 22–27 to be fibril-prone (43), PASTA indicates that also regions involving residues 2–10 are prone to aggregation. The many molecular configurations shown on Figure 5, could very well be the basis for the many morphologies observed for glucagon. It is, however, also possible that the packing of the residues outside the backbone region of protofilaments contribute to the general polymorphism of glucagon fibrils (18).

The fibril backbone residues can be probed by biophysical methods, including point mutations (43), hydrogen exchange (46), and enzymatic digest (47, 48). Pedersen *et al.* (2006) made an extensive work to find the fibrillogenic residues of glucagon (43). Fifteen carefully chosen residues were substituted for Ala and the affect on fibrillation kinetics examined by thioflavin T (ThT) fluorescence in a fluorescence plate reader. The main observation was that both N- and C-terminal patches are important for fibrillation. More specifically, they observed that residues Phe-6, Tyr-10, Val-23, and Met-27, when point mutated to an Ala, decrease fibrillation rates drastically. Other point mutations affected the fluorescence spectrum of

the fibrils without having a strong effect on fibrillation kinetics, a behaviour attributed to the general polymorphism of glucagon. Based on their observations, the authors proposed a loop model for glucagon, in which residues 6-12 form an anti-parallel β -sheet with residues 21-27 (or residues 6-10 and 23-27 if we include only the highly fibrillogenic residues found in the study). PASTA does allow for the peptide to form a β -sheet with itself in a loop structure, but the proposed loops have unfavourable energies compared to the energies of the arrangements shown in Figure 5, and in fact does not include the two regions proposed by Pedersen *et al.* (2006).

It is likely that the experimental conditions (salts and agitation) used in the experiments by Pedersen *et al.* (2006) favour a variety of morphologies with some morphologies having a backbone composed of N-terminal residues and some of C-terminal residues. In this way, N-terminal Ala substitutions only decrease the growth of a set of the morphologies present, and C-terminal Ala substitutions affect another set of morphologies.

2.4 Fibrils are built from protofilaments

In this and the following section, the structure of fibrils is outlined from the structure observed by TEM to the atomic-resolution structure.

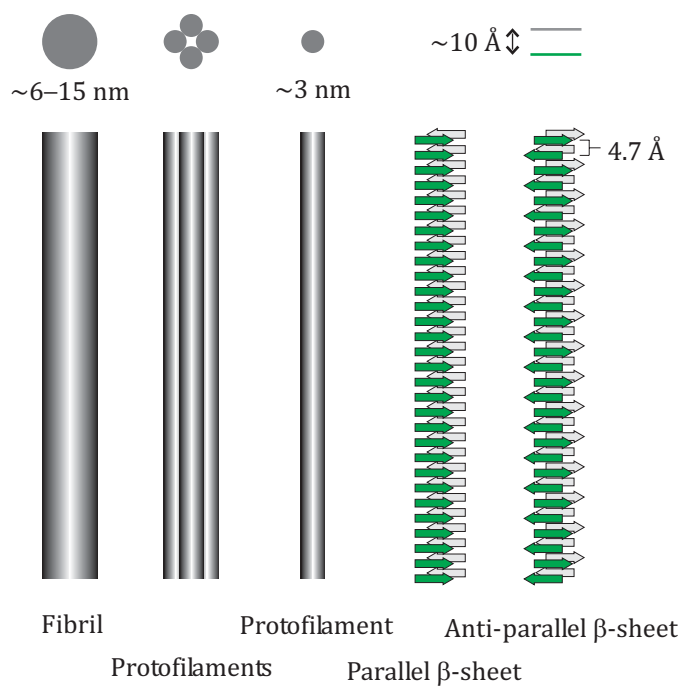


Figure 6. Schematic presentation of structure and nomenclature of a mature fibril. A typical fibril has a width of 6–15 nm, and is essentially an assembly of protofilaments each with a width of approximately 3 nm. A protofilament is a double-pleated β -sheet, which can be either parallel or antiparallel. The inter-strand distance is 4.7 Å and the inter-sheet distance is around 10 Å. Adapted from reference (49).

Figure 6 shows the overall structure of a fibril. The backbone of the fibril is defined as the amino acids forming a double-pleated β -sheet (indicated by arrows in the figure). The β -sheets can be either parallel or antiparallel to each other as indicated by the direction of the arrows in the figure. The distance between the individual β -strands is 4.7 Å and the inter-sheet distance is typically in the order of 10 Å. The inter-sheet distance correlates with the size of the amino acid residues and can hence vary significantly (50). The double-pleated β -sheet structure is referred to as a protofilament and often has a width around 30 Å (49). Protofilaments can assem-

ble in various ways and hence form a mature fibril. It is the exact arrangement of protofilaments that determine the morphological phenotype observable by TEM.

It is still controversial whether fibril polymorphism reflects the various ways identical protofilaments can assemble laterally, or whether it reflects polymorphism at a protofilament level. In fact, it seems likely that both views are represented in nature (18). Krishnan and Lindquist (2005) recently observed structural differences in the amyloid core of the yeast prion Sup35 (51). Two fibril strains formed at 4 °C and 25 °C, respectively, differed in terms of stability and length of the amyloid core. This experiment demonstrates that Sup35 fibril morphologies reflect protofilament polymorphism. In other studies, *e.g.*, a high resolution AFM study by Anderson *et al.* (2006), it has been observed that a fibril can change morphology during growth (52). This indicates that these fibrils are essentially an arbitrary assembly of identical protofilaments or rather that structural differences between protofilaments can be very subtle and allow for assembly into various fibril morphologies. Finally, in other cases, dichotomous branching, a process where a fibril splits into a number of sub-fibrils during growth without increasing the net number of protofilaments, has been observed (52-57). Hence, protofilaments may be only weakly bound together and can give rise to a number of morphologies. In summary, we have two (not mutually exclusive) views on the nature of fibril polymorphism: (a) differences in protofilament structure give rise to different morphologies, or (b) fibril morphologies result from the self-association of identical protofilaments. These views are summarized in Figure 7.

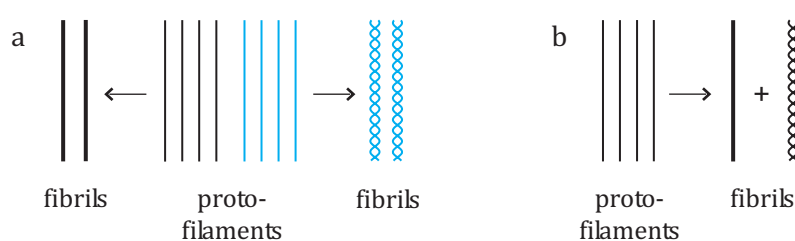


Figure 7. Assembly of fibrils from protofilaments. (a) Fibril polymorphism is the result of polymorphism of the protofilaments. The black and blue lines represent structurally distinct protofilaments, which form straight and twisted morphologies, respectively. (b) A population of identical protofilaments gives rise to polymorphic fibrils.

For glucagon, a great number of morphologies have been identified and classified by both TEM and AFM (17, 54, 57). As is often the case with fibril morphologies, the

growth conditions have a great impact on the distribution of morphologies present (17). Pedersen *et al.* (2006) identified four structurally distinct morphologies, whose population were apparently determined by the experimental conditions including salts, agitation, pH, and peptide concentration (17). As was observed during the Ph.D. study at hand, changing the peptide concentration in small steps from 0.25 to 8 mg/mL gradually changes the fibrils from having a predominantly twisted morphology to an almost completely homogeneous, straight morphology (19). In an interval, both morphologies are present. The ability to select morphologies was exploited to obtain an understanding of which scenario in Figure 7 best describes glucagon's polymorphism. In all experiments described in this thesis, glucagon powder was dissolved in 50 mM glycine/HCl pH 2.5 at 21 °C and agitation was kept to a minimum.

2.5 Fibril structure at atomic resolution

In recent years, significant advances have been made in understanding the structural organization within amyloid fibrils. The goal is to be able to determine the structure at atomic resolution, and to that end a number of different biophysical techniques have been applied. Insight into the structural basis for amyloid fibrils could lead to an understanding of the basis of structural polymorphism, and possibly devise new ways to control fibril growth.

Some of the first insights came from three-dimensional image reconstruction of a large number of cryo-EM pictures of mature fibrils as demonstrated by Saibil's group in 2002 (58). By reconstructing the three-dimensional structure of insulin fibrils of 2, 4 or 6 protofilaments, they proposed that insulin fibrils are built from arrangements of identical protofilaments and proposed a model of the protofibril based on a flat β -sheet structure between individual insulin molecules. The protofilament model is visualized docked inside the electron density reconstruction of a mature fibril in Figure 8a.

Additional insight came from solid state nuclear magnetic resonance (ssNMR). Measurements of dipole-dipole couplings between pairs of nuclear spins serve as molecular rulers indicating which ^{13}C and ^{15}N are close in space. Through *intermolecular* couplings, it is possible to obtain information about which part of the molecule has a cross- β structure, while *intramolecular* couplings put constraints on the secondary motifs at specific sites. In this way, ssNMR was the basis for creating a detailed model of A β (1-40) fibrils by Tycko *et al.* (2003) as demonstrated in Figure 8b (59). Approximately the first ten residues are structurally disordered in accor-

dance with observations showing these residues to be susceptible to proteolysis (32, 60). Residues 12-24 and 30-40 form two separate β -strand segments connected by a loop region. A single protofilament with a width of approximately 6 nm is made from two cross- β units in a parallel configuration as shown in Figure 8b. The core is mainly stabilized by hydrophobic interactions and more importantly by the fact that charged side chains are exposed to the solvent.

The most detailed understanding of the fibril backbone structure has been obtained by designing short fibrillogenic peptides known to be involved in the backbone region of various proteins. The short peptides are fully incorporated into the β -sheet backbone structure, and produces very well-ordered monomorphic fibrils, which readily form small crystals. Makin *et al.* (2005) used a small 12-mer polypeptide to study the basis of amyloid fibril structure (61). The peptide formed well-ordered fibrils, which readily formed nanocrystals. Using electron diffraction in combination with fiber diffraction, space group and unit cell dimensions were assigned to the crystal structure. Using these constraints, the peptide was modelled in a β -sheet conformation inside the unit cell, and it was shown that simulated diffraction patterns of the theoretical structure were similar to the experimental diffraction patterns. The structure revealed an antiparallel β -sheet zipped together by π - π bonding of the Phe rings on opposite strands and by salt-bridges between charge pairs of Glu and Lys.

In recent years, a large number of fibrillated polypeptides have been shown to form microcrystals. The group of David Eisenberg solved the structure of such microcrystals by X-ray diffraction at the microfocus beamline at ESRF, Grenoble (62, 63). Based on 13 such structures, they proposed a general scheme of backbone organization. The backbone consists of a pair of identical β -sheets formed by extended strands of the polypeptide, all perpendicular to the fibril axis. The two sheets meet at a dry interfaced, *i.e.*, an interface depleted from water and solvent molecules. The interface is essentially a tight intermesh of residues forming a steric zipper. The steric zippers formed eight groups depending on, *e.g.*, parallel/antiparallel configuration and the orientation of the surface of the sheets (face-to-face vs. face-to-back).

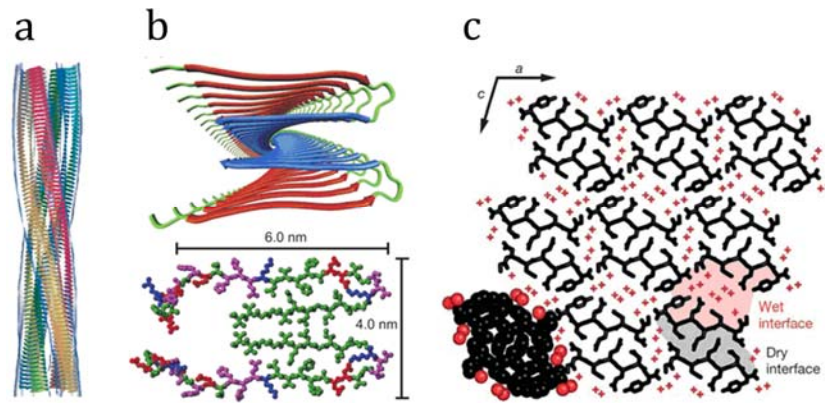


Figure 8. Fibril models obtained by different biophysical techniques. (a) Insulin fibril model based on cryo-EM and three-dimensional image reconstruction. Each protofilament has been assigned a color. (b) Aβ(1-40) fibril model viewed down the fibril axis based on ssNMR. (c) Fibril model of GNNQQNY based on X-ray diffraction on microcrystals. The picture shows nine β-sheets down the fibril axis. Reprinted from reference (58), (59), and (62), respectively.

Considering the recent significant advances in determining fibril structure at a molecular level, the first full-length structures solved at atomic resolution are within reach.

2.6 Fibril criteria

The highly ordered repetitive structure of the fibril backbone can be probed by a number of biophysical techniques. Traditionally, for fibrils stained with the sulfonated azo dye Congo red, the appearance of an apple green birefringence when observed under crossed polarizers was considered fingerprints of amyloid fibrils. Today, three biophysical criteria are considered essential for the classification of *in vitro* aggregates as fibrils: (i) the observation of fibril-like structures by TEM, (ii) X-ray fiber diffraction, and (iii) the binding of fibril-specific dyes, primarily ThT. In the following three sections, the basic principles of these criteria are explored using examples from the present work on glucagon fibrils. As will become clear, not only do these techniques help determine if a fibrous material is indeed amyloid fibrils, they also give insight into the structure of the fibrils and help elucidate even slight differences between morphologies.

2.6.1 Transmission electron microscopy

When viewed by TEM, fibrils often appear as micrometer long nonbranched structures built from subunits arranged as twisted ropes, ribbons, or bundles (3). The structures are typically highly organized with persistence lengths in the micrometer regime (64).

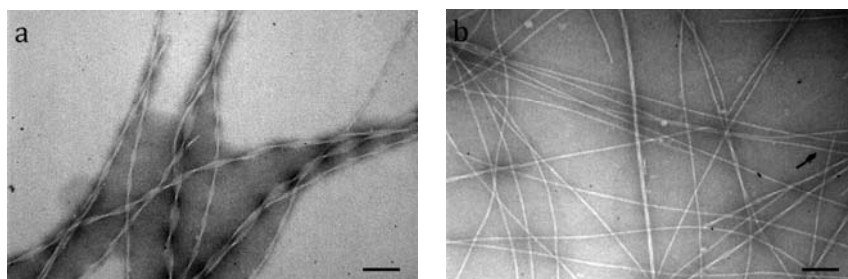


Figure 9. TEM pictures of glucagon fibrils formed at two different peptide concentrations: (a) 0.25 mg/mL and (b) 8 mg/mL. At 0.25 mg/mL, the fibrils share a morphology characterized by two or more protofilaments twisting around each other. At 8 mg/mL, the fibrils are predominantly straight and made up of two protofilaments. Bars represent 100 nm.

Figure 9 shows examples of TEM pictures obtained from fibrillated samples of 0.25 and 8 mg/mL glucagon (19). The fibrils are micrometers long and appear non-branched. The two TEM pictures also demonstrate fibril polymorphism, a phenomenon first reported for glucagon by Glenner *et al.* (1974) (65). The fibrils formed from 0.25 mg/mL of glucagon all share a twisted morphology with two or several protofilaments twisting around each other (Figure 9a). Put in more stringent terms, at 0.25 mg/mL of glucagon, the fibrillated sample is composed of a number of different morphologies, which all feature protofilaments with a repetitive twist. At 8 mg/mL, glucagon forms fibrils composed of a single protofilament, and the population of fibrils is very homogeneous (Figure 9b) (19).

Phenotypes observed by TEM are one way to identify differences in morphologies. It should be noted, however, that subtle structural differences between morphologies do not necessarily manifest themselves in TEM pictures, in which case other biophysical techniques should be applied (17).

2.6.2 Fiber diffraction

The highly repetitive pattern in fibrils can be probed by fiber diffraction (technique detailed in Chapter 6.2) (66). A fiber is a macroscopic partly aligned assembly of fibrils formed by various specialized techniques as summarized in reference (67). Often fibers are formed by letting a hanging drop of fibril solution dry from the ends of two wax-sealed end-to-end pipettes (68). When exposed to an X-ray beam, the characteristic distances in the fibrils will fulfil the Bragg diffraction condition and give rise to circular diffraction patterns (69). The characteristic distances are the meridional inter-strand distance of 4.7 Å and the equatorial inter-sheet distance of approximately 10 Å (49). Sometimes, other distances are found in the diffractogram, *e.g.*, related to the width of the smallest repeating unit, the unit cell, and distances related to the inherent twist of protofilaments (70). For the two glucagon morphologies observed by TEM in Figure 9, the diffractograms shown in Figure 10 were observed.

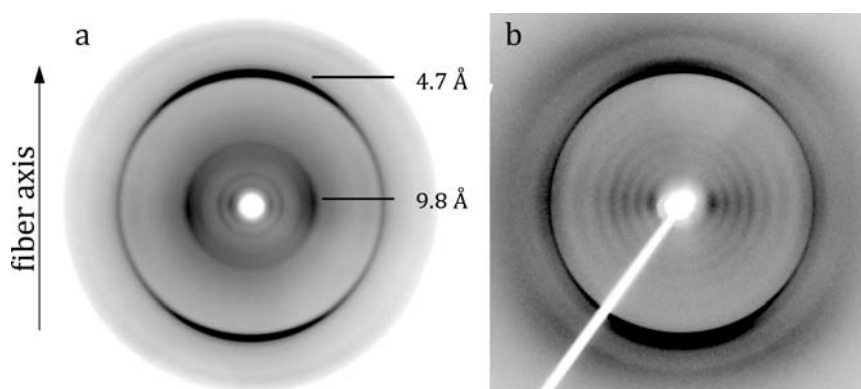


Figure 10. X-ray diffractograms of partially aligned glucagon fibrils. (a) 0.25 mg/mL fibrillated glucagon. The characteristic cross- β diffraction signal on the meridian and equator at 4.7 and 9.8 Å, respectively, are shown. (b) 8 mg/mL fibrillated glucagon.

Both diffractograms have a strong reflection on the meridian at 4.7 Å, as expected for the inter-strand distance in the β -sheet backbone, and a strong reflection around 10 Å due to the inter-sheet distance.

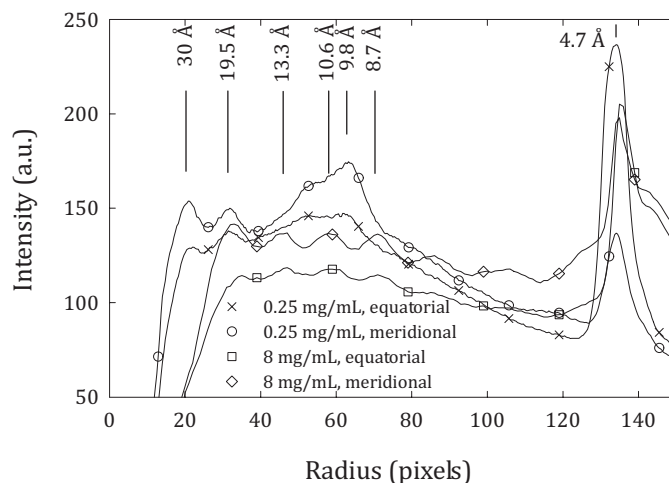


Figure 11. Intensity profiles of the glucagon fiber diffractograms in Figure 10. Intensity profiles were calculated by integration over a 60 deg angle along the equator and meridian, respectively. Approximate distances are shown in the plot.

A number of other reflections are also seen, although their physical origin is not easily interpreted. In Figure 11, the intensities along the radius of the detector, as obtained by integrating a 60 degree angle along the meridian and the equator, respectively, are plotted. The diffractogram from the twisted fibrils (Figure 10a) has a reflection around 30 Å, and this reflection could be related to the width of a single protofilament (cf. Figure 6). The diffractogram from the straight morphology fibrils (Figure 10b) has three peaks around 10 Å on the equator (8.7, 10.6, and 13.3 Å). The two diffractograms in Figure 10 are currently being analyzed by the use of the program CLEARER developed by the group of Dr. Louise Serpell (71).

2.6.3 Fibril-specific fluorescent dyes

A number of fluorescent dyes including ThT and Congo red have been shown to preferentially bind to the mature fibril structure (72, 73). The exact binding mechanism is not known, but due to its specificity toward fibrillar structures, it is expected that binding occurs in the regularly spaced grooves of the backbone (74).

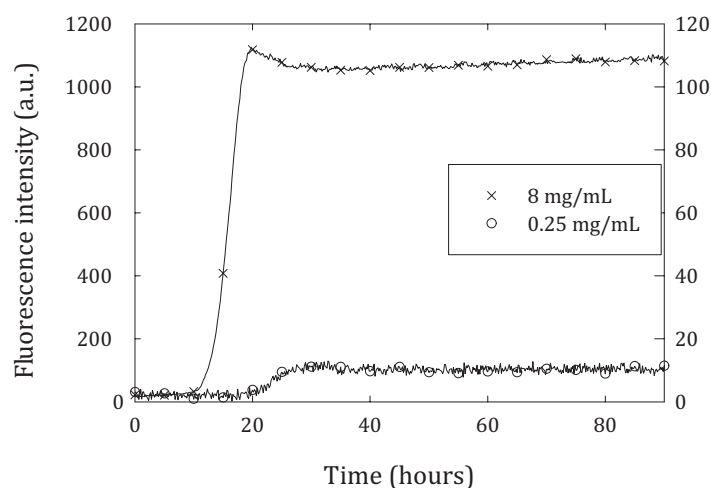


Figure 12. ThT fluorescence (plotted on separate axes) from 0.25 and 8 mg/mL glucagon during fibrillation. The fluorescence from the straight morphology fibrils formed at 8 mg/mL (left axis) is 100x higher than the fluorescence from the twisted morphology fibrils formed at 0.25 mg/mL (right axis). As the difference in concentration is only 32-fold, this demonstrates that ThT fluorescence is morphology-dependent.

Figure 12 shows the fibril formation of 0.25 and 8 mg/mL glucagon monitored by ThT fluorescence. After approximately 10 h, the fluorescence intensity from the 8 mg/mL solution increases abruptly and reaches a plateau within 10 h. In the case of the 0.25 mg/mL solution, the increase in intensity occurs after 20 h and within 10 h a plateau is reached. The increase in ThT fluorescence was shown by TEM to correlate with the appearance of significant amounts of fibrils (19). The fibrillation curves reflect an important property of ThT, namely that the fluorescence intensity depends on the morphology. In Figure 12, the intensity is 100-fold higher for the straight morphology (8 mg/mL) compared to the twisted morphology (0.25 mg/mL), a difference the 32-fold difference in concentration cannot account for (17).

2.7 *Intrinsic Trp fluorescence*

In this and the following two sections, three experimental techniques are presented, which all give structural information of the fibrils: Intrinsic Trp fluorescence, linear dichroism (LD), and proteolytic digest. The end result is a “collage” of information, which can be put into a picture of the fibril structure. Examples from the present work on glucagon will be shown along the way.

As the inherent fluorescent signal of aromatic residues Trp, Tyr, and Phe depends strongly on the environment, these residues can be used as intrinsic fluorescent probes of protein conformation, dynamics, and intermolecular interactions (75). Of the three, Trp is most frequently used, and this residue is often used to probe the conversion of proteins into fibril structures. When incorporated into the fibril structure, the fluorescence spectrum of the Trp residue is typically blue-shifted from a maximum around 350 nm to approximately 320 nm. The ratio between the peak maxima is therefore often used to probe fibrillation kinetics (76).

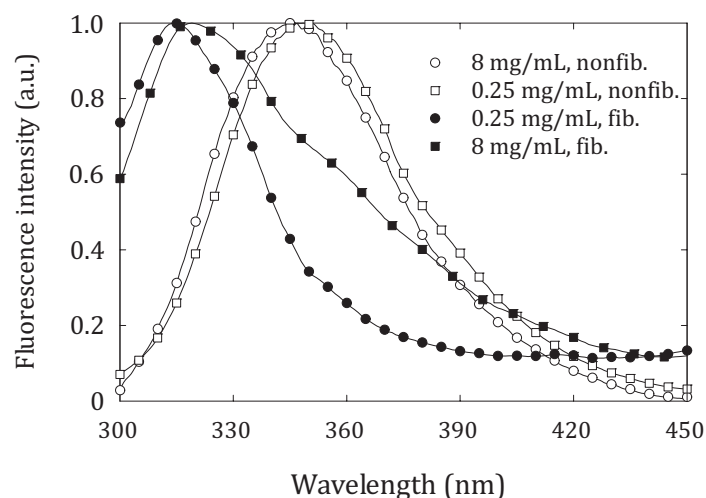


Figure 13. Fluorescence spectra of freshly prepared 0.25 and 8 mg/mL glucagon samples (open symbols) compared with fibrillated samples formed at identical peptide concentrations (solid symbols). The nonfibrillated 0.25 and 8 mg/mL samples have maxima at 348 and 346 nm, respectively. The fibrillated 0.25 and 8 mg/mL samples have a maxima at 314 and 319 nm, respectively, and the Trp residues are thus significantly blue-shifted when incorporated into the fibril structure. The fibrillated 8 mg/mL sample was diluted 32 times to take the difference in concentration into account and data has been normalized. Excitation wavelength $\lambda_{\text{ex}} = 290$ nm.

Glucagon contains a single Trp residue, Trp-25, and using this residue it is possible to study glucagon fibrillation kinetics without adding fluorescent dyes (17, 19). Figure 13 shows fluorescence spectra of fibrillated samples of 0.25 and 8 mg/mL glucagon from 300–450 nm when excited at 280 nm. The spectra are compared with spectra of freshly prepared, nonfibrillated samples of 0.25 and 8 mg/mL glucagon,

which have maxima at 348 and 346 nm, respectively. The spectrum of fibrils formed at 0.25 mg/mL is significantly blue-shifted with a maximum at 314 nm, and similarly, the spectrum of the fibrils formed at 8 mg/mL has a maximum at 319 nm. This demonstrates the sensitivity of the Trp residue to the surroundings.

2.8 Linear dichroism

The polarization of light is often applied to probe molecular structure. Left and right circularly polarized light, for example, interacts differently with chiral molecules and secondary structure elements giving rise to small differences in the fraction of absorbed light (77). This effect is explored in circular dichroism (CD) and can give information about the structural content of proteins (19). Linear dichroism (LD) is a technically related method relying on differences in absorption of linearly polarized light in horizontal and vertical direction, respectively (78). Only samples oriented in a specific direction will display linear dichroism. For fibrils and DNA, this is possible after alignment in a flow cell. LD can provide information about the presence of secondary structure elements, α -helices and β -sheets, and the relative position of the aromatic residues including Tyr and Trp (78). The LD technique has in recent years been applied to amyloid fibrils by Dafforn *et al.* (2004) and Adachi *et al.* (2007) (79, 80). Dafforn *et al.* (2004) compared CD and LD spectra of various fibrous materials and found that A β (1-42) fibrils have strong positive peak around 200-205 nm characteristic of fibers with a β -sheet structure more perpendicular than parallel to the fiber axis (79). No signal was observed in the aromatic region (250-300 nm) despite a high content of Tyr and Phe. Adachi *et al.* (2007) flow-aligned fibrils of a fragment of β_2 M, which forms two different morphologies. The spectra showed strong absorbance differences in the aromatic region. The aromatic signal was assigned to a Tyr residue in the peptide, which was shown to have its transition moment oriented in parallel to the fibril axis.

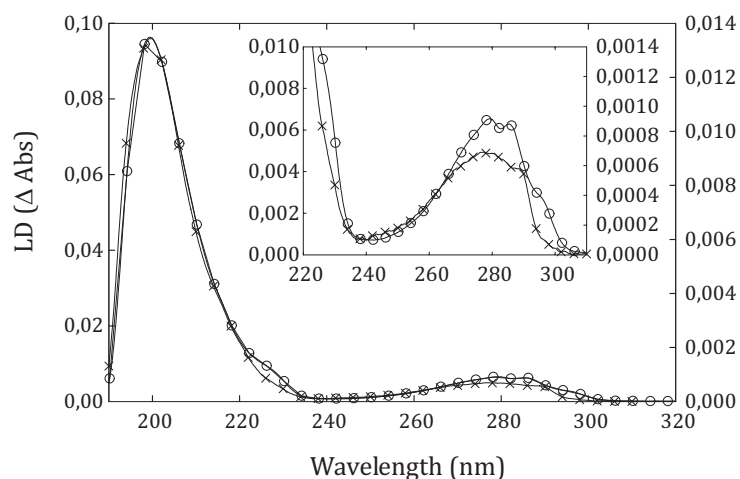


Figure 14. LD spectra from 190–320 nm of flow-aligned straight (○) and twisted (×) fibrils (plotted on left and right axis, respectively). The inset shows the aromatic region in detail. The fibrils formed at 8 mg/mL were diluted 32x to take the difference in concentration into account.

LD spectra of flow-aligned glucagon fibrils formed under the two conditions central to this Ph.D. project have been measured by Dr. Matthew Hicks, University of Warwick, and they are shown in Figure 14. The figure shows the LD spectra from 190–320 nm of flow-aligned twisted and straight fibrils. A shoulder around 230 nm for the straight morphology and a large spectral difference in the aromatic region (inset) stands out. The twisted morphology fibrils have a pronounced shoulder at 287 nm, which is absent in the straight morphology. This could suggest more conformational freedom of the Trp-25 residue in the straight morphology. The shoulder at 295 nm is also likely to be due to the orientation of the Trp-25 residue and may be related to the shoulder at 230 nm. The fibrillated 8 mg/mL sample was diluted 32x to take the difference in concentration of the two samples into account, but still the LD signal is 7–10x higher for the straight morphology sample. Although data analysis is currently in progress, it is clear that the structural differences of the twisted and straight morphologies also manifest themselves by LD.

2.9 Proteolysis of fibrils

The fibril core is often very stable and resistant to proteases. This property has been exploited to determine the regions forming the β -strands perpendicular to the fibril axis (47, 48). Typically, the mature fibrils are digested by adding pepsin. The enzyme chews off all residues not protected in the fibril core, and leaves the fibril

backbone intact. The fragments released by the enzyme are removed by repeatedly isolating the fibrils by centrifugation, removing the supernatant and rediluting in buffer. The fibrils are dissolved and separated by size or hydrophobicity. In one particular study, two different fibril morphologies of β_2M were found to have different digest patterns when digested by pepsin (48).

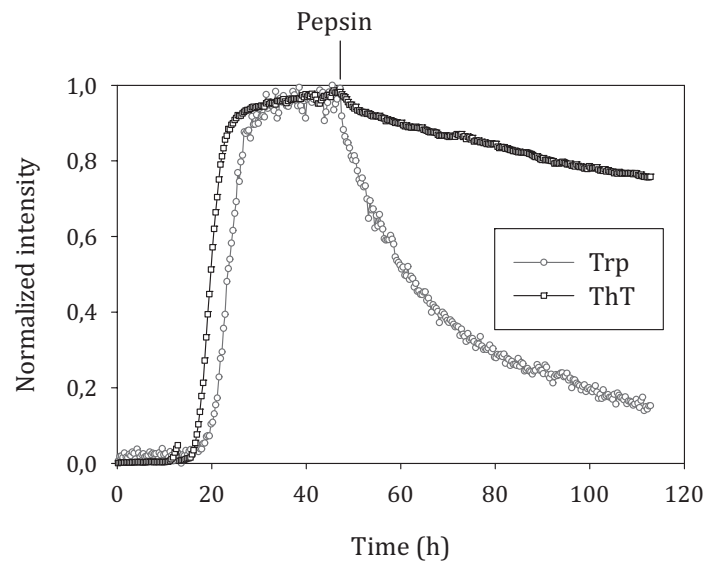


Figure 15. Fibrillation of glucagon and subsequent pepsin digest of the fibrils formed followed by ThT and Trp fluorescence. After 60 h, the ThT signal is essentially unchanged, but the Trp signal has decreased to approximately 15 % suggesting that the fibrils are intact but the Trp-25 has been cleaved off.

Glucagon fibrils of straight and twisted morphology were digested in order to determine if the morphologies are due to differences in the amino acid stretches forming the amyloid core. The PASTA algorithm described in Section 2.3 predicts that this could indeed be the case. Unfortunately, only the straight morphology fibrils are protease resistant. Figure 15 shows the fibrillation of 8 mg/mL of glucagon followed by ThT and Trp fluorescence. After approximately 50 h, pepsin is added to the fibrillated sample solution. The ThT fluorescence is essentially unchanged even after 60 h, clearly demonstrating that fibril structures are still present. The Trp fluorescence, on the other hand, is simultaneously decreased to approximately 15 % of the initial level hereby showing that pepsin has had an effect on the peptide, and that probably the C-terminal has been affected.

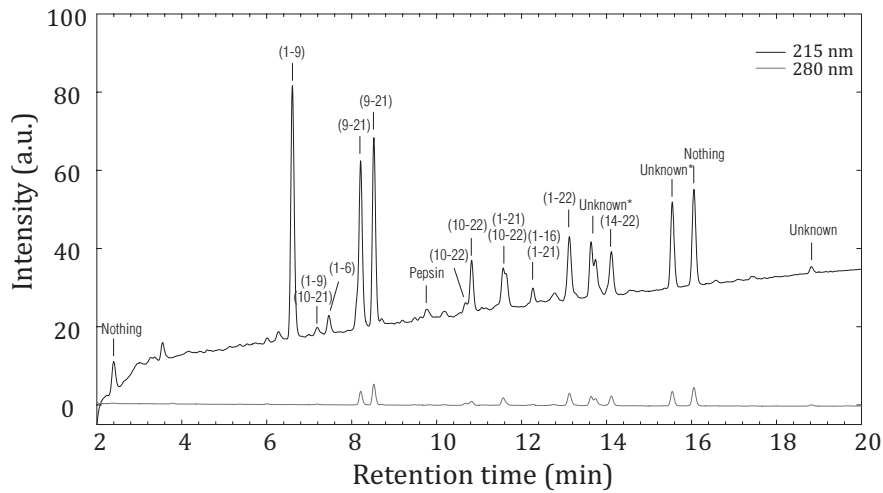


Figure 16. Identification of the fibril core. After pepsin digest, the pepsin-resistant fibril core was isolated, dissolved, and separated by RP-HPLC. Each peak was identified by MS and shown to belong to residue 1-22 of glucagon. Two peaks of equal mass were not identified, but do probably belong to pepsin itself.

The peptide core was separated by RP-HPLC as shown in Figure 16. Of the 16 peaks, three were unidentified, but probably belong to pepsin itself. The remaining peaks all belong to glucagon residue 1-22. Residues 23-29, including Trp-25, were never observed in accordance with the observed change in Trp fluorescence upon digestion. The fragments identified are shown in Figure 17 sorted descending according to the area of the peaks in Figure 16.

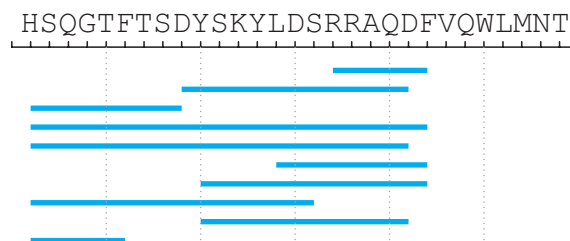


Figure 17. Fragments in the fibril core sorted descending according to the peak area. All fragments belong to residue 1-22 of the glucagon peptide.

This chapter has shown that fibrils formed from either 0.25 or 8 mg/mL of glucagon have different morphologies. Structural differences were revealed through TEM, fiber diffraction, ThT fluorescence, Trp fluorescence, LD, and proteolytic digestion.

More work is necessary to conclude that hydrogen-bonding in two different parts of the glucagon peptide gives rise to the two morphologies described above. However, based on the biophysical data at hand, it is clear that significant structural differences characterize the two morphologies studied, and these differences are likely to result from polymorphism in the protofilaments involved. The work on glucagon presented in this chapter is currently being prepared for publication. It is surprising that changing the concentration of glucagon molecules in the test tube has such a profound impact on the fibril structure. In the next chapter, the mechanism behind this selection of morphologies is explored.

3. Selection of morphologies

In this chapter, the mechanism behind the selection of morphologies is examined through cross-seeding experiments and insight into the self-association of glucagon in solution.

3.1 Templated fibril growth

A special class of experiments are designed to explore the properties of fibrils in terms of growth kinetics, the so-called seeding experiments. As will become clear in the following, seeding experiments can be useful in characterizing differences in morphology. The basic principle behind seeding is based on the assumption that new fibrils can form by templated growth from fragmented fibrils as sketched in Figure 18.

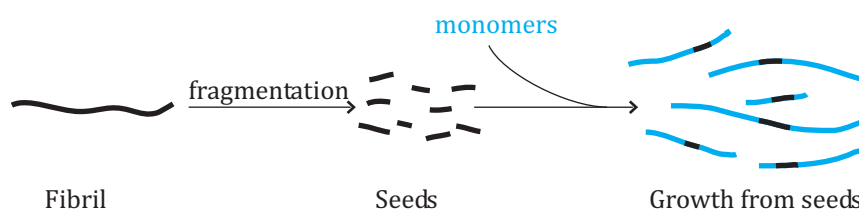


Figure 18. The principle of seeded fibrillation kinetics. Seeds are formed by fragmentation of fibrils from an already fibrillated sample. When added to a fresh solution of protein, seeds act as templates for continued growth.

A fibrillated sample is fragmented by sonication or mechanical stress, and seeds are formed. When added to a freshly prepared peptide solution, minute amounts of seeds act as templates and initiate fibril growth from the seed ends. We distinguish between self-seeding and cross-seeding depending on whether or not the growth conditions are identical to the conditions the seeds were formed under. Self-seeding experiments bypass the often long lag phase dominated by spontaneous nucleation and hence focus on the fibril elongation process. In a later section (Section 4.7), it will be described how self-seeding can be used as a method to shed light on the very nature of the fibril growth mechanism. Cross-seeding experiments determine if a given morphology can sustain growth under conditions different from the original seed conditions. In this way, Yagi *et al.* (2005) demonstrated that α -synuclein can be seeded by fibril seeds from hen lysozyme, *E. coli* chaperonin GroES, and bovine insu-

lin (81). In each case, it was demonstrated that the seeds were incorporated into the mature fibrils. This rather extreme example of cross-seeding demonstrates the versatility of the fibril backbone to template fibril growth, even when the incoming monomer is completely different from the protein at the seed end. This property arises from the fact that fibrils predominantly assemble through amino acid backbone interactions rather than side chain interactions (82). If the seed ends are not receptive to monomers, seeding has no effect on the lag phase.

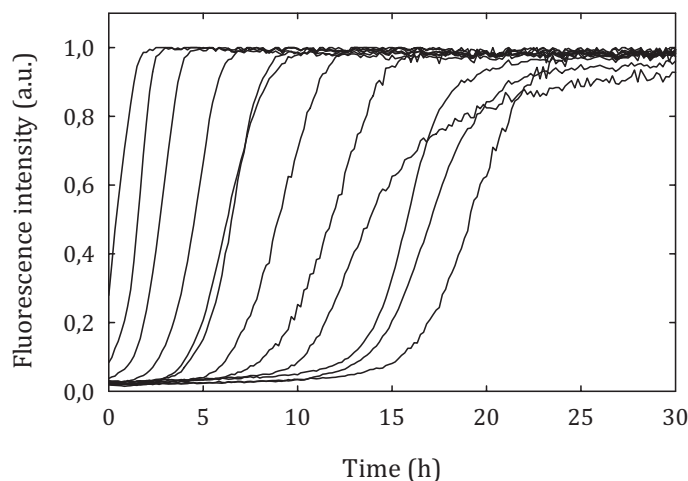


Figure 19. Seeded fibrillation kinetics. An 8 mg/mL glucagon solution is seeded with seed concentrations ranging from 10⁻³ to 400 μ g/mL with intermediate concentrations separated by a factor of 5. The rightmost curve is the nonseeded kinetics. As the seed concentration is increased, the lag phase is decreased. The intensity was normalized with respect to the maximum fluorescence intensity.

Self-seeding and cross-seeding experiments were performed by adding minute amounts of twisted and straight seeds to freshly prepared 0.25 and 8 mg/mL glucagon solutions. An example of seeded fibrillation of an 8 mg/mL glucagon solution is shown in Figure 19. The resulting kinetics profiles were characterized by the duration of the lag phase as detailed in reference (19). Considering the experiments by Yagi *et al.* (2005), it is expected that both fibril morphologies would sustain growth when cross-seeded. After all, the change in glucagon concentration should only impact the fibril growth rate.

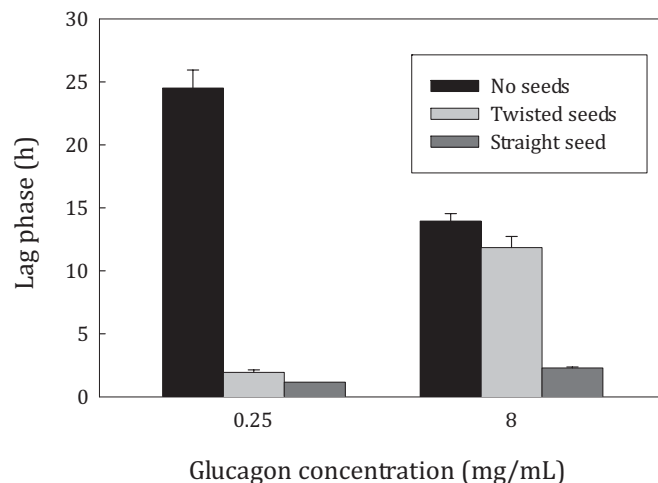


Figure 20. Seeding 0.25 and 8 mg/mL glucagon solutions with pre-formed seeds formed at either 0.25 mg/mL (twisted seeds) or 8 mg/mL (straight seeds). Seeds of either morphology have a profound effect on the lag phase when added to a 0.25 mg/mL sample solution, and so do straight seeds when added to an 8 mg/mL sample solution. Puzzling, twisted seeds have no effect when added to an 8 mg/mL glucagon solution. The seed concentration was approximately 3 $\mu\text{g/mL}$.

The lag phases of the seeding experiments are shown in Figure 20. At a seed concentration of approximately 3 $\mu\text{g/mL}$, the lag phase of the 0.25 mg/mL solution is reduced from 24 h to 1.2 and 1.9 h when self-seeded and cross-seeded, respectively. The 14 h lag phase of the 8 mg/mL solution is reduced to 2.3 h upon self-seeding, but when cross-seeded, the reduction in the lag phase is negligible and within the error margin. An effect, if any, could be caused by the small fraction of straight fibrils present in fibrillated 0.25 mg/mL samples. The morphology of the seed-induced fibrils were subsequently determined by TEM as shown in Figure 21.

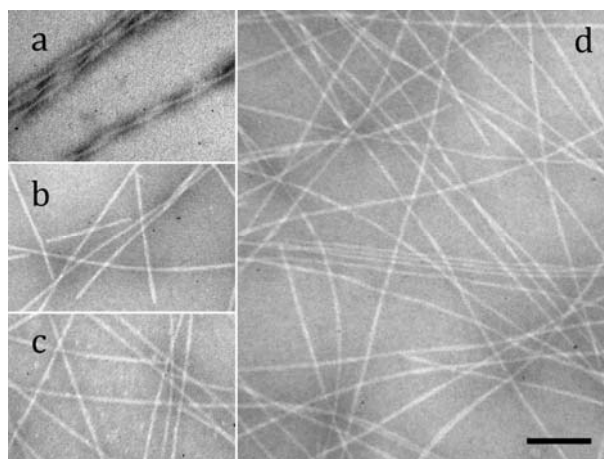


Figure 21. Morphologies of fibrils after the seeding experiment shown in Figure 20. (a) 0.25 mg/mL self-seeded. (b) 8 mg/mL self-seeded. (c) 0.25 mg/mL cross-seeded. (d) 8 mg/mL cross-seeded. In accordance with Figure 20, the twisted seeds added at 8 mg/mL sample solution has no effect on the resulting morphology. Bar represents 100 nm. From reference (19).

Figure 21a and b show that self-seeding conserves the morphology imprinted by the seed. Figure 21c shows that straight seeds when added to a 0.25 mg/mL glucagon solution conserves the morphology of the seeds. Intriguingly, the twisted seeds do not imprint their morphology when added to a fresh solution of 8 mg/mL glucagon. In conclusion, cross-seeding twisted seeds to an 8 mg/mL sample solution, where straight fibrils dominate under non-seeded conditions, has no effect on neither lag phase nor morphology. The origin of this peculiar behaviour is detailed in the next section.

3.2 Morphology-dependent growth inhibition

In a series of fibrillation experiments, freshly prepared solutions of 0.25–8 mg/mL glucagon were fibrillated at 21 °C in a fluorescence plate reader. Intuitively, increasing the peptide concentration should increase the fibril growth rate as the monomers are not as easily locally depleted at the growing fibril ends. Fibrillation kinetics were characterized by an hour long lag phase followed by a rapid increase in fibril mass (19). The lag phase was calculated for each sample and is plotted as a function of the peptide concentration in Figure 22.

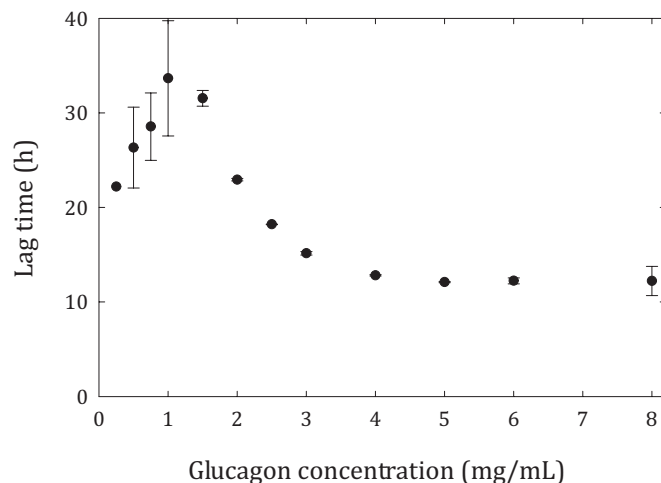


Figure 22. Lag phase duration as a function of the peptide concentration. The maximum at 1 mg/mL stands out. From reference (19).

The lag phase plot in Figure 22 shows that as the peptide concentration is increased from 0.25 mg/mL to 1 mg/mL, the lag phase *increases* from approximately 22 to 34 h. Above 1 mg/mL, a further increase in peptide concentration decreases the lag phase until it reaches a plateau around 12 h at high concentrations. The behaviour when gradually increasing the concentration from 0.25 mg/mL to 1 mg/mL stands out. In a separate experiment, the experiment above was repeated and samples examined by TEM as soon as the maximum fluorescence level had been reached (19). Interestingly, as the peptide concentration is increased from 0.25 mg/mL, the fraction of straight fibrils increase at the expense of twisted fibrils. Above 2.5 mg/mL the straight fibril morphology is by far the most numerous with only minute amounts of nonstraight fibrils.

In search for an explanation for the peculiar lag phase behaviour, the self-association of glucagon molecules in freshly prepared solutions was examined by a light scattering method devised by Glatter (83, 84). The glucagon oligomer size as a function of the peptide concentration is plotted in Figure 23.

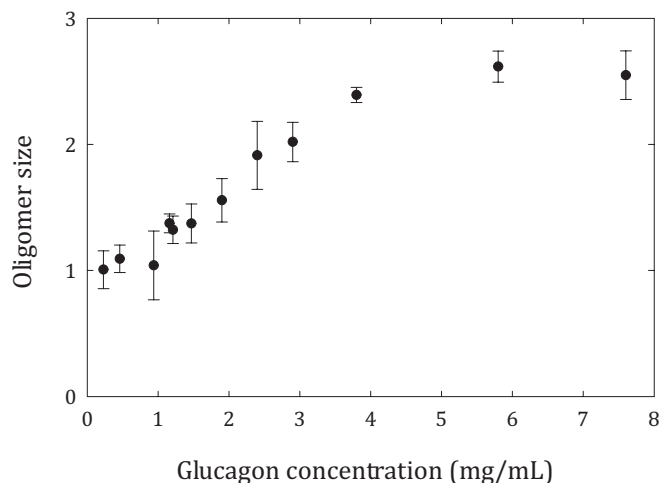


Figure 23. Concentration-dependent self-association of glucagon. At low concentration, glucagon is predominantly monomeric, and at high concentration, glucagon forms trimers. From reference (19).

The figure demonstrates that glucagon is monomeric at low concentration and has an oligomer size of 2.6 at high concentrations. This suggests a monomer–trimer equilibrium under the solvent conditions used throughout this study. The trimer conformation has been confirmed in previous studies under different solvent conditions (85, 86), and also by the fact that the crystal structures of glucagon are trimeric (85, 87). By singular value decomposition of CD spectra, it was established that the monomer–trimer equilibrium does not involve a significantly populated dimer state (19).

Based on the correlation between the increase in the lag phase and the formation of glucagon trimers, we hypothesise that the trimer is able to specifically inhibit the twisted morphology fibrils. So in summary, at low concentrations of glucagon, the twisted morphology dominates. As the peptide concentration increases, so does the fraction of reversible trimers, and these trimers have the ability to specifically block twisted fibrils from growing. With the twisted fibrils struggling to grow, another morphology, the straight morphology, becomes the most numerous. As straight fibrils are not blocked by trimers, a further increase in peptide concentration decreases the lag phase (Figure 22). Turning to the seeding experiments shown in Figure 20, we propose that the surprising behaviour observed when cross-seeding twisted fibrils to an 8 mg/mL glucagon solution is due to the inhibition of twisted fibrils by reversible trimers as summarized in Figure 24.

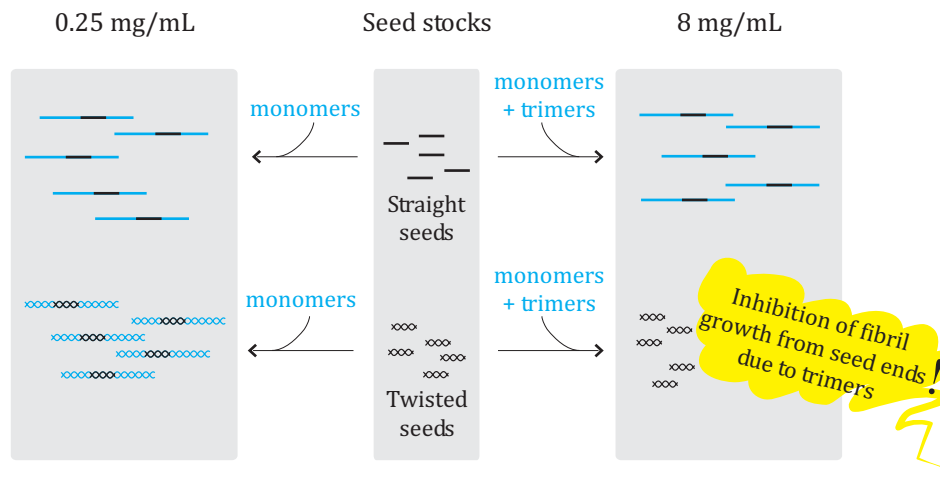


Figure 24. Inhibition of twisted fibrils by reversible trimers. Seeds formed by fragmentation of straight fibrils decrease the lag phase when added to fresh solutions of glucagon at either 0.25 or 8 mg/mL. At the same time, the seeds determine the morphology at either glucagon concentration. In contrast, seeds from twisted fibrils readily self-seed, but fail to increase the fibrillation rate at 8 mg/mL glucagon. Instead, the fibrils formed have the straight morphology expected for non-seeded solutions of 8 mg/mL glucagon. We conclude that growth of twisted fibrils is inhibited by reversible trimers, and hypothesise that reversible trimers are able to bind to the ends of twisted fibrils.

The exact molecular mechanism behind the inhibition of fibril growth by reversible trimers remains unanswered. Recent experiments by Hong *et al.* (2006) demonstrate that the inhibition of fibril growth due to oligomers may be a general phenomenon (88). In their study, they observed slowing of fibrillation of the insulin B-chain when increasing the concentration from 0.2 to 0.5 μM . At higher concentrations, no fibrillation was detected, and this anomalous behaviour was attributed to the formation of oligomers with increasing concentration. In the case of the insulin B-chain, the oligomers preferentially form protofilaments instead of mature fibrils. Devlin *et al.* (2006) studied insulin fibril growth and found that adding preformed seeds of either insulin A-chain or B-chain both resulted in a reduced lag phase, but also that the fibrils formed were morphologically different from the seeds (89). In a separate experiment, self-seeded insulin fibril growth was shown to be inhibited by the soluble form of insulin A-chain and B-chain peptides, respectively. They were, however, able to show that the inhibition was due to interaction between the A-

chain and the B-chain, respectively, with the soluble form of insulin, rather than through interactions with the seed ends.

4. Fibrillation kinetics

Fibrillation kinetics describes the rate of change of fibrillar species. Fibrillation experiments performed *in vitro* are often characterized by a long lag phase, in which apparently only minute amounts of fibrils are formed, followed by a sudden increase in fibril mass. Curiously, amyloid diseases are also characterized by a very long incubation period—sometimes decades long—followed by a rapid development of disease phenotype (11). The disease phenotype is believed to be connected to the accumulation of fibrils or fibril-related species (10, 11, 90, 91). In this chapter, the current understanding of this kind of kinetics is detailed with emphasis on recent experiments obtained during this Ph.D. work, which elucidates the kinetics mechanism responsible for glucagon’s sigmoid reaction profile.

4.1 Nucleation-dependent aggregation

In solution, a fibril can form by spontaneous nucleation from monomers. Once formed, the nucleus elongates into a fibril by continuous addition of monomers. Spontaneous fibril formation is sketched in Figure 25.

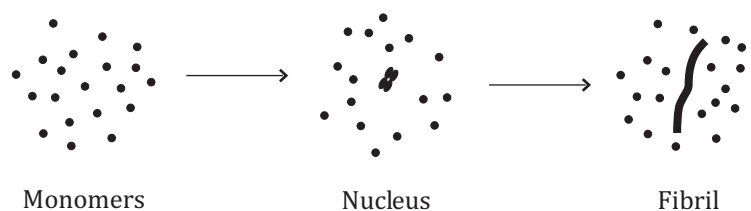


Figure 25. Spontaneous formation of fibrils. A fibril nucleus is in equilibrium with monomers. Once formed, the nucleus gives rise to the formation of a fibril.

Fibrillation kinetics are often characterized by a sigmoid reaction profile, in which a long lag phase is followed by a phase of fast fibril mass accumulation. During the lag phase, only minute amounts of fibrils are formed, hence the lag phase is often used as a qualitative measure of the fibrillation propensity of a protein. The physical interpretation of the lag phase is complex. In one view, a number of different oligomeric species are formed during the lag phase until finally a sufficient number of nuclei have formed to initiate rapid fibril growth (92). In an opposite view, the lag phase is due to the inherent ability of fibrils to produce new fibrils with

a rate proportional to the already formed fibril mass giving rise to exponential mass growth (93, 94). These two views are summarized in Figure 26.

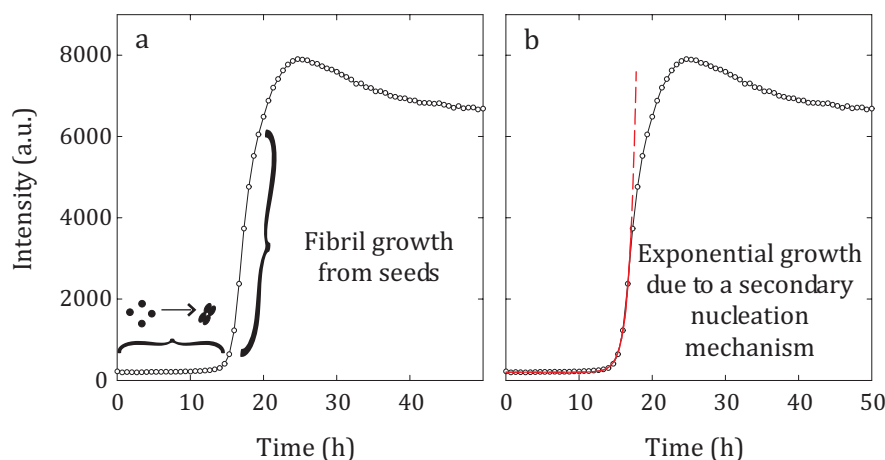


Figure 26. Two opposing views on the typical fibrillation profile. (a) The lag phase represents the nucleation phase and when a number of nuclei have accumulated, a phase of rapid fibril elongation follows. (b) The sigmoid reaction profile is due to a secondary nucleation mechanism forming new fibril ends in proportion to the fibril mass already present thus increasing fibril mass exponentially (93, 94). Both figures show fibrillation of an 8 mg/mL solution of glucagon, and in (b) an exponential of the form $I(t) = a \exp(bt) + c$ was fitted to the initial part of the curve, where the intensity was less than 35 per cent of the maximum intensity.

4.2 Oligomeric species and protofibrils

During fibril formation, metastable intermediates are commonly observed. These intermediates may be in the form of small oligomers or protofibrils (18, 90, 91, 95). Generally, oligomers are considered small ensembles of monomers, which may or may not be in equilibrium with monomers or other oligomeric species (18). When examined by TEM, AFM, or light scattering, oligomers often appear small and spherical when compared to protofibrils and fibrils. Protofibrils are defined from their appearance when examined by TEM or AFM, where they often appear non-spherical elongated structures without a periodic substructure. Structural order seems to increase from oligomers to protofibrils to fibrils (18). Protofibrils may resemble rod-like or worm-like fibrils, and in this case a lower ThT fluorescence signal or fiber diffraction is used to distinguish the two different structures (68).

Gosal *et al.* (2005) monitored the aggregation of β_2 -microglobulin (β_2 M) by AFM under different experimental conditions (ionic strength, pH, and protein concentration), and found data suggesting the existence of two competing pathways (96). One pathway is non-nucleated and gives rise to oligomers and kinetically trapped protofibrils, while the other is nucleation-dependent and leads to mature fibrils. In other words, the β_2 M-protofibrils do *not* mature into fibrils and neither are they on the reaction pathway to fibrils. Instead, the aggregates and protofibrils are formed through a mechanism very different from that of fibrils, namely downhill polymerization, which does not require a nucleation step (93, 94, 97). In downhill polymerization, the polymer is formed by addition of monomers through a series of successive steps. Using electrospray ionization mass spectrometry, Smith *et al.* (2006) showed that under conditions favouring β_2 M protofibril-formation, oligomers of sizes up to 11-mers were found, while under conditions favouring mature fibrils, only dimers to tetramers were detected (98). In general, oligomers and protofibrils are most often considered to be off-pathway, owing perhaps to experimental difficulty in obtaining quantitative data to make tight kinetic arguments, and most data are inconsistent with the hypothesis that such species are on-pathway (18). Two recent studies using small-angle X-ray scattering (SAXS) and small-angle neutron scattering (SANS) have studied the size and shape of oligomeric species present at early time-points in protein solutions (99, 100). In the SAXS study by Vestergaard *et al.* (2007), the early elongation events of insulin fibrils formed above the critical concentration was studied *in vitro*. Three major components were identified: monomers, mature fibrils, and a homogeneous population of oligomers composed of five to six monomers. As the elongation rate was found to be proportional to the concentration of oligomers, the authors proposed a dual role of the oligomers: as a structural nucleus—the starting point of new fibrils—and as the smallest unit in fibril elongation (99). Although the notion that mature fibrils elongate by addition of oligomeric species is conceptually new and would need confirmation by different methods, the experiments show the power of SAXS to detect and model oligomeric species involved in fibrillation.

A special interest in prefibrillar or side-product structures formed during the fibrillation process is due to their possible connection to the onset of clinical symptoms in amyloid and prion diseases (10, 11, 101). As several subtypes of neurodegenerative diseases have been identified, it has become apparent that the severity of symptoms of the respective diseases is not linked quantitatively to the amount of fibrillar deposits accumulated in neural tissue. Perhaps even more intriguing, some

amyloid and prion diseases do not show fibrillar aggregation, while at the other extreme, amyloid plaques are found throughout the cortex of many cognitively normal 70-year-olds (10). These findings suggest that the oligomers or protofibrils observed *in vitro* are correlated to the disease progression rather than the mature fibrils.

Two AFM studies of fibrillating glucagon solutions have been carried out by separate groups and both reported oligomeric species in samples at early time-points (54, 57). As time progresses, structural order increases as protofilaments and later mature fibrils are formed, leading the authors of both studies to suggest a mechanism, in which protofilaments are formed from oligomers, and the mature fibrils are subsequently formed by lateral assembly of protofilaments.

4.3 Secondary nucleation mechanisms

Spontaneous fibril growth is very often characterized by a long lag phase followed by fast formation of fibril mass. As explained in a detailed review by Ferrone (1999), this behaviour cannot simply be explained by a nucleated growth mechanism, where the lag phase is ascribed the slow formation of a rare nuclei species, from which the mature fibrils are subsequently formed by fast monomer addition to the ends (94). Instead, two other reaction schemes within nucleation-dependent aggregation have been proposed to describe the origin of the lag phase (93). In the first scheme, the nucleus is formed through a number of successive steps, and once formed, the nucleus gives rise to mature fibrils through addition of monomers to the seed ends. If the number of steps is sufficiently large, a prolonged lag phase is predicted. Flyvbjerg *et al.* (1996) successfully modelled the assembly of microtubulin—a process which involves a pronounced lag phase—by proposing a model involving a nucleus of 15 heterodimers (102). A second scheme relies on fibril-dependent nucleation, in which the presence of fibrils increase the chance that new fibril ends are formed in a manner proportional to the fibril mass present. This creates an exponential growth in fibril mass (93, 94, 103). Fibril-dependent fibril formation is believed to occur through one of the following three mechanisms: surface-dependent fibril formation, fragmentation, and branching (94). These fibril-dependent nucleation mechanisms—usually referred to as secondary nucleation mechanisms—are illustrated in Figure 27.

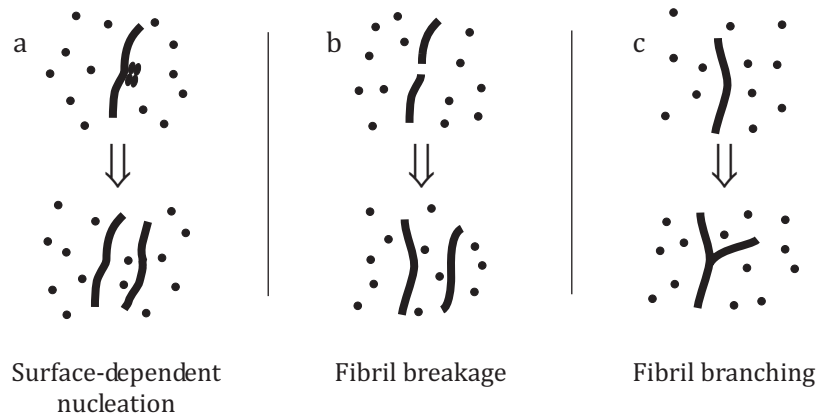


Figure 27. Three different secondary mechanisms are shown. (a) Surface-dependent nucleation denotes a process, in which nucleation is enhanced at the surface of a fibril. After a while, the nucleus dissociates and gives rise to a new fibril. (b) In fibril breakage, a fibril breaks due to stress or thermal fluctuations hereby exposing two new fibril ends. (c) Fibril branching denotes a process, where a new fibril protrudes from the side of an existing fibril. In all three cases, the result is the formation of new fibril ends from existing fibrils.

Common to secondary mechanisms is the generation of new fibril ends from existing fibrils. In this way, the increase in fibril mass is proportional to the fibril mass already formed and hence the kinetics become exponential (93, 94). So far, experimental evidence for these mechanisms has been scarce. Ruschak and Miranker (2007) studied fibril-dependent nucleation of residue 20 to 29 of IAPP in the presence and absence of a CH_2Cl_2 :aqueous interface where primary and secondary nucleation, respectively, are the dominating nucleation processes (104). They found that primary and secondary nucleation could be modeled by the same mechanism and concluded that the secondary nucleation process need not be different from spontaneous nucleation. Hence, the secondary nucleation involved in IAPP fibrillation could be surface-dependent nucleation (Figure 27a). In another experimental work on insulin, Smith *et al.* (2006) determined the nanoscale properties of single fibrils (105). They determined the breakage rate due to thermal fluctuations, and found that fibril breakage (Figure 27b) could be the secondary mechanism accounting for the sigmoid reaction profile found during insulin fibrillation (92). In the following section, it is demonstrated that fibril branching (Figure 27c) accounts for the sigmoid reaction profile of glucagon.

4.4 Glucagon fibril branching in surface layers

In the light of the overall picture just described, the remainder of this chapter will discuss the implications of my own results on glucagon. TIRFM is a specialized fluorescence microscopy technique that enables real-time observations of fibril growth in an approximately 150 nm thin layer close to the quartz surface (106). The technique is detailed in Section 6.1. The TIRFM technique has been optimized for the study of amyloid fibril growth in the lab of Dr. Yuji Goto, which also applied the technique to seeded reactions of A β (1-40) and β_2 M (107-109). The primary observation in these experiments is that the amyloid fibrils grow exclusively by addition of monomers to fibril ends. In a series of experiments, fibril growth of seeded solutions of 0.25 mg/mL glucagon was monitored by collecting images of the surface layer at fixed intervals. An example of such a real-time movie is attached on a cd-rom (Supplementary Movie). Three close-ups from the movie are shown in Figure 28.

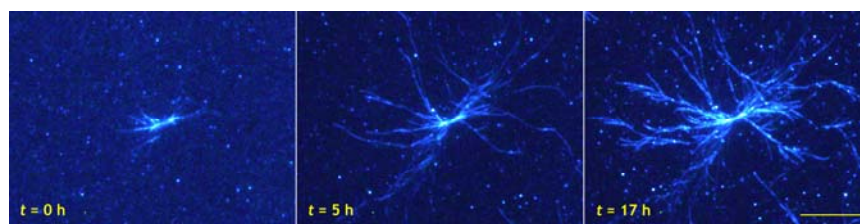


Figure 28. Three pictures showing glucagon fibril growth at times specified on the figure. After 5 h, fibrils have grown up to 25 μm in length, and new fibrils have formed by branching. After 17 h, a relatively dense spherulitic structure has formed. The bar represents 10 μm .

During the experiment, fibril grows radially from clusters of seeds, and most notably, new fibril ends are formed continuously by branching until a large spherulitic structure with a diameter of 40–50 μm has formed. Rogers *et al.* (2006) studied insulin spherulite formation by optical microscopy and found that over time the density of the spherulites grew linearly or faster, indicating that the space fills as the spherulites grow (110). This observation, they proposed, could be due to extensive branching of insulin fibrils during growth. Our TIRFM observations of glucagon fibrils forming dense spherulites support this proposal.

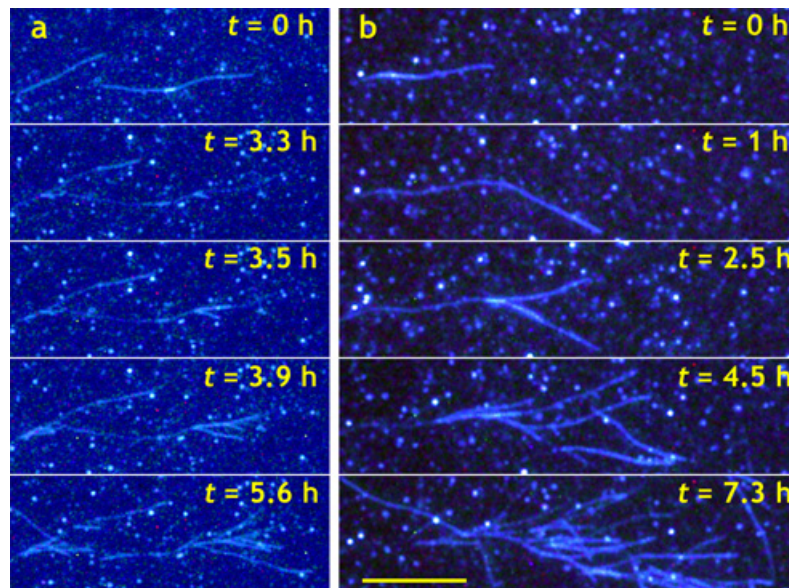


Figure 29. Branching detail from two separate experiments. (a) Two fibrils grow from seeds in the center of the picture. At $t = 3.3$ h, a branching event along the fibril is observed and in the following hours, several such events are observed. (b) A fibril grows from a seed in the left hand side of the picture. After 1 h, the fibril forms a kink and in the following hours a fibril is formed close to the kink ($t = 2.5$ h). Finally, a cascade of new fibrils is formed, and at $t = 7.3$ h, fibrils branching off from fibrils formed by branching themselves are observed. The bar represents $10 \mu\text{m}$.

Figure 29 shows two examples of branching events from separate experiments. In Figure 29a, two fibrils grow in opposite directions from a small cluster of seeds. While this could be interpreted as bidirectional growth, it should be noted that the optical resolution does not allow for a distinction between single seeds and clusters of seeds. In fact, most often single fibril growth in only one direction was observed. (data not shown). After 3.5 h, a new fibril is formed by branching and this process repeats itself in the following hours resulting in several new fibrils. In one case, a fibril grows along the parent fibril for a few micrometers before leaving at an angle. In Figure 29b, a fibril is seen growing along the surface. At one point it forms a kink, and in the following measurements several fibrils protrude close to the kink. Branching did not occur close to growing fibril ends, and a single fibril were often observed to branch into several new fibrils, showing that the observed phenomenon is not untwisting of intertwined protofilaments.

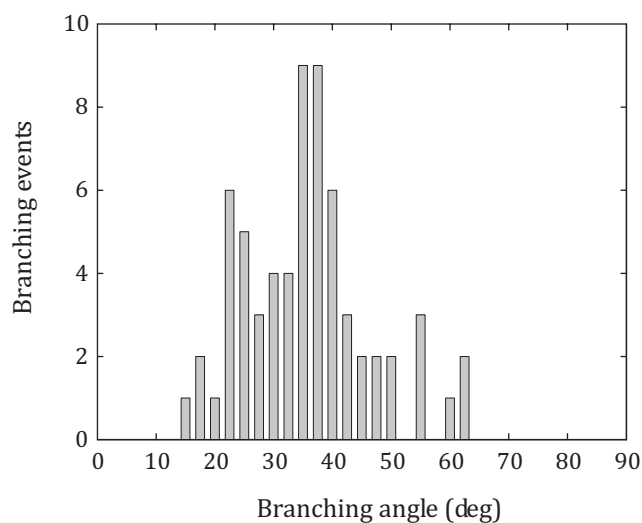


Figure 30. Distribution of branching angles measured with respect to the direction of growth of the parent fibril. 65 branching events on a single slide glass were measured. Branches most frequently form an angle of 35–40 deg and branching opposite the direction of growth is never observed.

In Figure 30, branching angles from a single experiment have been binned and plotted in a histogram. Branching angles fall between 15–65 deg, and the distribution is approximately symmetric with a maximum at 35–40 deg. Even more significantly, branching events were exclusively in the direction of growth. However, in a number of cases, the newly formed fibril grew along the parent fibril for several micrometers before leaving at an angle. These zero-angle events have not been included in the branching angle histogram.

One interpretation is that glucagon fibrils are polar structures with growth in only one direction. If branches develop from surface-dependent nucleation on a polar surface, a particular direction of branching could be preferred. Goldsbury *et al.* (1999) and Blackley *et al.* (2000) have reported bidirectional fibril growth using time-lapse Atomic Force Microscopy (AFM) studies (55, 111). However, Goldsbury *et al.* (1999) reported that higher-order Islet Amyloid Polypeptide (IAPP) fibrils often appeared blocked at one end (55). Glucagon fibrils formed under the conditions used in this study are also higher-order, composed of two or several protofilaments with a repetitive twist (19). Another possibility is that branches grow from defects that are created during the growth process, and therefore have a preferential angle relative to the direction of growth. The observation that branches

often protrude close to kinks (Figure 29) seems to support this possibility, although surface-dependent nucleation on a polar fibril might also be enhanced at kinks. Defects might form during growth by untwining of single protofilaments from the main bundle, which then continues to grow. Later, the dangling protofilaments matures to a growing fibril. A number of groups have reported fibrils splitting into protofilaments during growth without increasing the net number of protofilaments (52-55, 57). Most studies are static measurements on fibrillated samples, but Goldsbury *et al.* (1999) described the same phenomenon using time-lapse AFM (55). Their data show an example of a protofilament growing out of a thicker fibril, which then continues growth in a different direction (Figure 3b of reference (55)). In order for an untwining mechanism to support continuous branching as shown in Figure 28 and Figure 29, the untwined protofilament must be replaced in the growing bundle, or the fibril would run out of protofilaments to untwine. A similar mechanism should exist to inflate the dangling protofilament to a full-size fibril, capable of forming new branches itself.

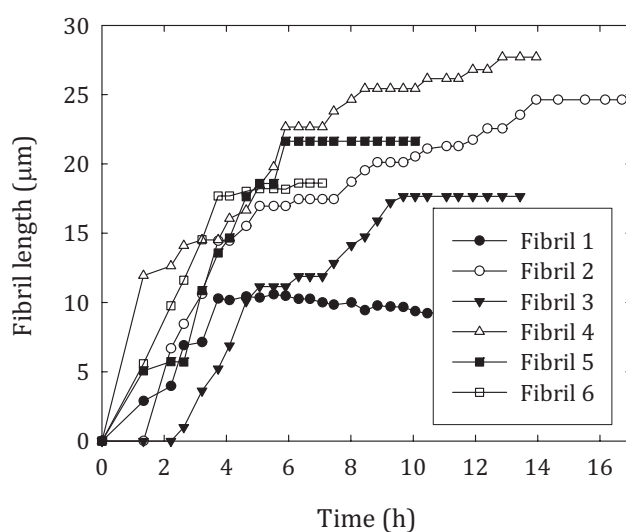


Figure 31. Length in μm of six individual fibrils from a single real-time measurement. Fibrils exhibited stop-and-run behaviour characterized by intervals where no growth occur followed by continued growth.

Six individual fibrils, which grew from the seeds added initially, were identified and their length measured. In Figure 31, the length of each fibril is plotted as a function of time. The final length of the fibrils ranged from 10 to 28 μm . Occasionally, the fibrils showed stop-and-run behavior, where a fibril after hours of continuous

growth stops growing for a while and then resumes growth. Also, two of the six fibrils stopped growing after less than four hours although fibrils in their vicinity kept growing for several hours (fibril 1 and 6 in Figure 31). While this could be due to a local depletion of monomers, the stop-and-run behavior could also be due to monomers misaligned at the fibril end. If this is the case, fibril growth would resume after the monomer had either aligned properly to the fibril backbone or dissociated from the fibril end. We also note that of the six fibrils, whose lengths were plotted in Figure 31, only two continue growth throughout the experiment (fibril 2 and 4). The others stop growing after 3.7–9.7 h. This could indicate that the fibril end of these fibrils have been terminated due to a misaligned monomer or perhaps due to morphology-dependent binding of a reversible glucagon trimer as proposed in Section 3.2.

4.5 TEM pictures of branching glucagon fibrils

Examination of fibrillated samples by TEM showed several examples of branched fibrils. As TEM sample preparation involves pipetting to a carbon-coated grid, staining, and drying of the sample, care should be taken when interpreting the results. Despite these reservations, we were able to identify a number of cases, where a single fibril branched into two or several fibrils. Four examples are shown in Figure 32. The fact that a single fibril was observed to branch into several fibrils, makes it less likely to be an artefact from sample preparation (Figure 32a). In some cases, the fibril split into two separate fibrils, which continued growth side by side (Figure 32d). While this could be due to the sample preparation, it could also be examples of the events observed by TIRFM, where newly formed fibrils grow along the parent fibril for several micrometers.

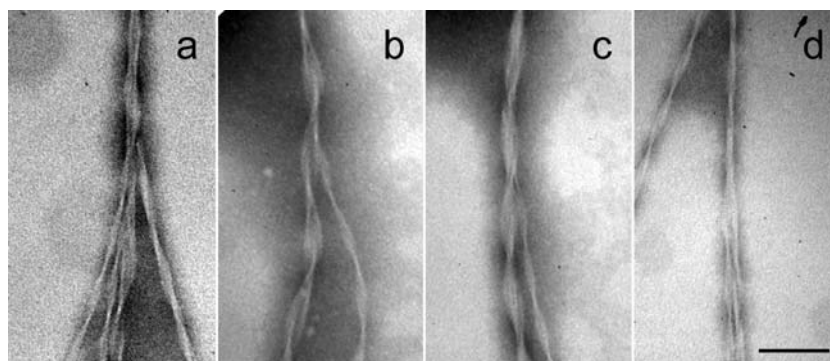


Figure 32. TEM pictures of branching fibrils. Most often, the fibril split into two fibrils (b-d), but in a some cases several fibrils branched off from the parent fibril (a). In (d), the fibril branches splits into two fibrils with a branching angle close to zero degrees. Scale bar represents 100 nm.

4.6 Kinetics in bulk solution

Light scattering measures fibrillation kinetics in solution and offers an opportunity to test if the branching observed by TIRFM on quartz surfaces also occurs in bulk solution. A small-angle light scattering (SALS) setup was designed specifically for studying the growth of large micrometer structures, in this case fibrils. The large-angle light scattering (LALS) setup measures the scattered intensity at $q = 23 \mu\text{m}^{-1}$ and is hence more sensitive to the growth of fibrillar species of smaller size. Experiments were performed on both light scattering setups simultaneously with aliquots from the same sample preparation. Generally, the light scattering signal from a solution increases, when the components aggregate to form larger structures such as fibrils. The light scattered at small angles from a solution containing various fibrillar species mainly comes from large structures, while smaller fibrillar species contribute relatively more at large angles. The scattered intensity is used as a qualitative measure for the growth in fibril mass, although it should be noted that the two are not directly proportional. For example, fibrils bundling together forming large structures can give rise to an increase in the scattered intensity, in particular at small angles, without an increase in fibril mass.

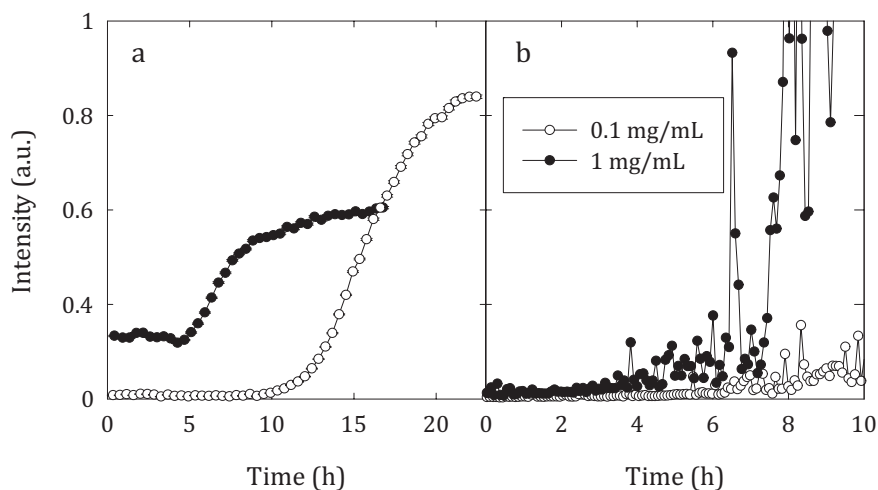


Figure 33. (a) Seeded glucagon kinetics monitored by SALS at $q = 0.84 \mu\text{m}^{-1}$ (1.8 deg). The reaction profiles are characterized by a long lag phase. Increasing the seed concentration ten-fold decreases the lag time from approximately 10 to 5 h. (b) Seeded glucagon kinetics monitored by LALS at $q = 23 \mu\text{m}^{-1}$ (90 deg). After a long lag phase, the intensity increases irregularly as large particles diffuse through the small scattering volume.

Figure 33a shows the scattered intensity at $q = 0.84 \mu\text{m}^{-1}$ (1.8 deg) from 0.25 mg/mL glucagon solutions seeded with 0.1 and 1 $\mu\text{g}/\text{mL}$ seeds as a function of time. At a seed concentration of 0.1 $\mu\text{g}/\text{mL}$, the beginning of the reaction profile is dominated by a long lag phase. After approximately 10 h, the scattered intensity increases abruptly and reaches a plateau at the end of the experiment. Increasing the seed concentration to 1 $\mu\text{g}/\text{mL}$ conserves the general reaction profile. The initial scattered intensity is higher suggesting that the signal at early times is mainly due to the seeds. The lag phase is reduced to approximately 5 h.

The scattered intensity at $q = 23 \mu\text{m}^{-1}$ from seeded solutions of glucagon is plotted in Figure 33b. After some hours with a relatively moderate increase in scattered intensity, the scattered intensity increases abruptly and fluctuates as large particles diffuse through the small scattering volume. This occurs after approximately 9 and 5 hours for seed concentrations of 0.1 and 1 $\mu\text{g}/\text{mL}$, respectively.

The prolonged lag phase followed by an explosive increase in fibril mass, as detected by SALS and LALS in Figure 33, is the hallmark of a secondary process. The light scattering data hence suggests that the secondary process observed at the quartz surface layer also takes place in solution.

4.7 Criteria for the existence of secondary nucleation mechanisms

The group of Dr. Goto previously measured TIRFM real-time growth of A β (1-40) from seeds at physiological pH (107). In contrast to glucagon fibrils, A β (1-40) fibrils grew exclusively by addition of monomers to fibril ends, and branching was not observed. This fundamental difference in fibrillation kinetics of the two peptides was exploited by making a comparison of seeded fibrillation kinetics in solution. A new method based on seeded fibrillation kinetics is devised in order to discriminate between fibrillation dominated by spontaneous nucleation and fibrillation dominated by secondary nucleation mechanisms.

Spontaneous nucleation. In seeded solutions of fibrils unable to generate new fibril ends by secondary nucleation mechanisms, fibril growth will initially be dominated by addition of monomers to a fixed number of fibril ends assuming that the spontaneous nucleation is a slow process compared to the fibril growth. The increase in fibril mass will be linear in time with a slope proportional to the number of seed ends:

$$[A_f]_{\text{spon}}(t) = k[E] \cdot t$$

where $[A_f]_{\text{spon}}$ is the concentration of fibril-bound monomers, k is a rate constant, and $[E]$ the seed concentration. This scenario is plotted in Figure 34a.

Secondary nucleation. Seeded solutions, in which fibrils are able to continuously generate new fibril ends from existing fibrils, have an exponential increase in fibril mass (93, 94):

$$[A_f]_{\text{sec}}(t) = k_1[E] \exp(k_2 t)$$

where $[A_f]_{\text{sec}}$ is the concentration of fibril-bound monomers, k_1 and k_2 are constants, and $[E]$ the seed concentration. Increasing the seed concentration will not affect the exponential nature of the growth, but does affect the lag phase (for details see Section 8.2). This scenario is plotted in Figure 34b. As stressed in Section 4.3, the lag phase in itself does not imply that a secondary nucleation mechanism is present; a sufficiently large nucleus formed by downhill polymerization will also give rise to a lag phase. However, in *seeded* fibril reactions, the lag phase does imply the existence of a secondary nucleation mechanism.

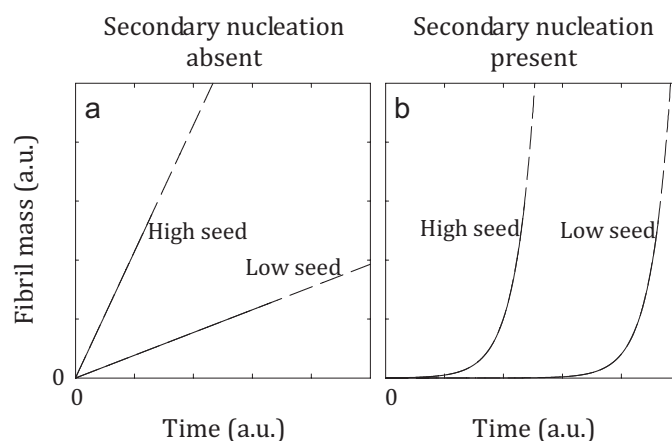


Figure 34. The effect of seeding fibril processes on the initial part of the fibrillation curve. (a) Seeding a kinetic process, which forms new fibril ends by spontaneous nucleation only, changes the growth rate. Increasing the seed concentration, increases the growth rate. (b) Seeding a kinetic process dominated by a secondary nucleation mechanism shortens the lag phase, but does not change the exponential nature of the growth (right panel).

The kinetics of seeded glucagon solutions were shown for two different seed concentrations in Figure 33a. In both cases, the kinetics were dominated by a long lag phase characteristic of exponential reactions followed by a rapid increase in fibril mass. We performed the same light scattering experiments on seeded solutions of $A\beta(1-40)$ reproducing the experimental conditions from the original TIRFM experiments (107). The data are shown in Figure 35. The $0.5 \mu\text{g}/\text{mL}$ seed concentration corresponds to the original seed concentration, and once again we compare against a ten times higher seed concentration to examine the effect of changing the seed concentration. The growth as measured by SALS and LALS was linear, and increasing the seed concentration increased the slope.

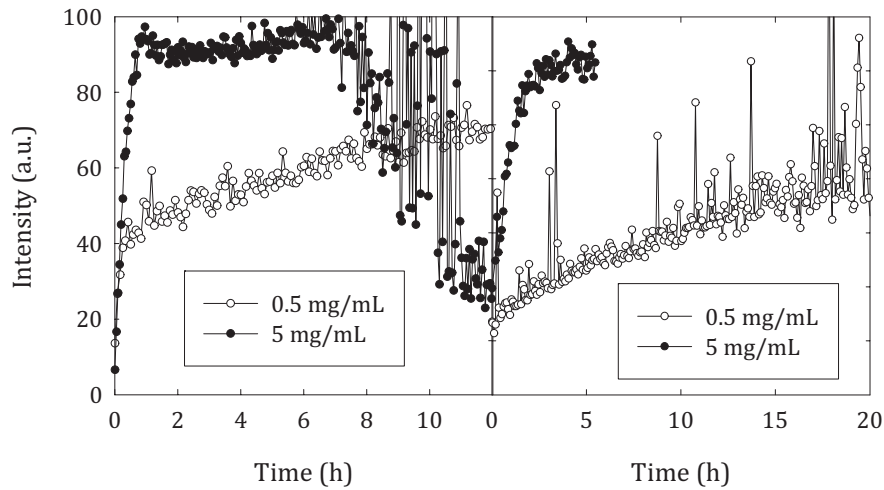


Figure 35. (a) Seeded $A\beta(1-40)$ kinetics monitored by SALS at $q = 0.84 \mu\text{m}^{-1}$ (1.8 deg). The fibril mass grows linearly, and increasing the seed concentration ten-fold increases the growth rate. (b) Seeded glucagon kinetics monitored by LALS at $q = 23 \mu\text{m}^{-1}$ (90 deg). The growth in fibril mass is similar to the signal at low angles.

In conclusion, by following the time-dependent fibril mass growth of seeded solutions, it is possible to determine if secondary nucleation processes are involved in the formation of fibrils. If the effect of adding seeds is to change the linear growth rate, secondary nucleation mechanisms are not involved. If increasing the seed concentration shortens the lag phase, secondary nucleation mechanisms do play a role. The light scattering data presented in Figure 33 and Figure 35 suggest that fibrillation of $A\beta(1-40)$ does not involve a significant contribution from secondary nucleation processes, while the opposite is the case with glucagon, and hence supports the TIRFM observations presented here and in reference (107).

5. Prion diseases

A group of lethal amyloid diseases are characterized by their ability to transmit between individuals. These are the so-called prion diseases. Prion diseases include bovine spongiform encephalopathy (BSE) in cattle, scrapie in sheep, and Creutzfeldt-Jakob's disease (CJD) in humans. In the mid-80's, certain European countries approved a new procedure to process carcasses for feed and as a consequence, a new strain of the hitherto rare prion disease BSE spread through cattle. Most notably in the UK where two million cattle became infected with the disease. Later it became clear that CJD—the human analogue of BSE—could be induced in humans, who had consumed prion-infected meat. So far, around 200 people have been diagnosed with this new variant CJD (vCJD) (11). Like other amyloid diseases, prion diseases have very long incubation periods followed by rapid progression of the disease phenotype. The BSE example illustrates two important properties of prions: they transmit within a species with relative ease, and sometimes they even cross the barrier between species.

Prion diseases are all related to a prion protein (PrP), a naturally occurring highly conserved glycoprotein, which in its soluble cellular form, PrP^c, is completely harmless to the cell. For long, it was widely accepted that PrP^c can be converted into a fibrillar form mediated by a PrP^c isoform denoted PrP^{Sc}, and it was hypothesised that the PrP^c and PrP^{Sc} isoforms differ only in the monomer conformation and aggregation state (112). However, recently, this hypothesis has been challenged, and it is now believed that the infectious entity is the ends of a small fibrillar form of PrP^c (11). However, very little is known about the structure of the infectious particle (101).

Probably the most interesting aspects of prion diseases are how a proteinaceous infectious entity encodes a strain with a specific disease phenotype, while it at the same time remains adequately unspecific in order for it to cross the species barrier by accepting foreign prion primary sequences. As it turns out, the encoding of strain properties is closely related to the structural properties of the fibrils, and the ability to cross between species is related to templated fibril growth detailed in Section 3.1. These properties are further detailed in Section 5.1 and 5.2 with emphasis on the analogy to the glucagon results presented in this thesis. Furthermore, the importance of secondary nucleation mechanisms on the strain phenotype and stability is detailed in Section 5.3.

5.1 Strain encoding

Fraser *et al.* (1973) isolated multiple strains of scrapie and propagated the strains in lines of inbred mice with identical PrP gene (113). The strains differed in terms of incubation period and neuropathology and remained stable when propagated. As the prion proteins in the experiment were identical, the strain properties must be encoded in the structure of the pathogenic fibrils rather than the primary structure. The fact that biologically different strains do indeed have different biophysical properties have since been shown for various prion proteins including human PrP^{sc} (114) and the yeast prion protein Sup35 (51). In both these studies, it was shown that the backbone region was structurally different for each strain, thus the connection between strain and fibril morphology was established. The fact that a proteinaceous entity is responsible for a variety of strains—and hence morphologies—makes it less likely that a single misfolded protein encodes such diverse information. Instead, it seems more likely that a small seed-like particle encodes the hydrogen bond pattern necessary for accepting prion monomers. This was demonstrated in a study by Silveira *et al.* (2005), in which the infectivity was examined on partly disaggregated PrP fibril samples fractionated by size and characterized by light scattering (101). Oligomers of less than six PrP peptides were substantially inactive, and instead non-fibrillar particles equivalent to 14-28 PrP molecules were the most efficient pathogenic species.

The glucagon seeding experiment detailed in Section 3.1 demonstrates that a straight morphology seed is able to imprint its own morphology under conditions which normally favours a different morphology. This is analogous to the concept of strains. In accordance with the results by Fraser *et al.* (1973), the two glucagon "strains" differed in terms of structure as well as kinetics.

5.2 Transmissibility

Another question that has been puzzling scientists for many years is the question as to how a prion disease crosses the species barrier. Essentially, crossing the species barrier refers to the ability of a prion strain to accept PrP with a different primary structure. For example, in experimental settings, the new strain responsible for the cattle BSE epidemic readily transmits to a range of species with different PrP primary structure. Remarkably, when transmitted back into cattle, the biological characteristics of the strain have been conserved (11). The situation is sketched in Figure 36.

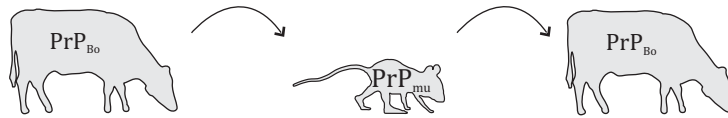


Figure 36. The BSE strain responsible for the new variant CJD in humans, vCJD, readily crosses species barriers, but maintains its biological characteristics upon passage through an intermediate species with a different PrP primary structure (here murine PrP). Adapted from reference (11).

A striking example of strain transmission came from studies of transmission of human prion diseases (115). The study focused on transmission of the classical CJD prion strain and the new vCJD prion strain. The two strains, which have identical primary structure, were propagated in wild type mice expressing murine PrP and transgenic mice expressing human PrP only. The classical CJD failed to transmit to wild type mice, but readily transmitted to humanized mice expressing human PrP. In contrast, vCJD, despite having a PrP primary structure identical to the PrP expressed in humanized mice, only transmitted efficiently to wild type mice. The study concluded that the prion strain type—not the primary structure—has the greatest impact on the transmission efficiency. The experiment, which suggests that the species barrier is actually better described as a transmission barrier, is summarized in Figure 37.

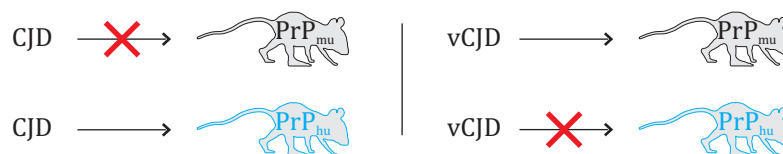


Figure 37. Species barrier vs. transmission barrier. Classical CJD strains do not transmit to wild type mice (black), but easily transmit to humanized mice expressing human PrP (blue). BSE-derived vCJD prions, despite having a primary sequence identical to the classical CJD, easily transmit to mice expressing murine PrP, but inefficiently transmit to humanized mice.

Two possible explanations to the observations in Figure 36 and Figure 37 have been proposed: (i) under certain conditions, a strain is composed of an ensemble of structurally distinct morphologies each with its own infectious entity PrP^{Sc}, or (ii)

the infectious entity of a certain strain is able to adopt a plethora of PrP primary sequences. The first explanation is analogous to the perhaps most striking observation of *in vitro* experiments; the observation that fibrils are composed of a large number of different morphologies some more predominant than others. If this scenario is also occurring *in vivo*, a strain should perhaps be visualized as a population of morphologies with the most frequent occurring being responsible for the biological phenotype. The role of the other morphologies could be manifested when the strain is introduced into a new host, in which case the morphology able to propagate in the new host will become the most dominant. The second explanation assumes that the infectious entity of certain strains is able to accept a wide diversity of monomer configurations, while other strains are more specific toward the monomer configuration. The strains capable of crossing species barriers may hence have an infectious unit with a hydrogen pattern capable of accepting protein backbones without being too restrictive with respect to the primary sequence. This situation is analogous to the cross-seeding experiments performed by Yagi *et al.* (2005), in which seeds of α -synuclein were capable of accepting a variety of proteins (see Section 3.1 for details) (81).

5.3 Strain stability

Amyloid diseases including prion diseases are characterized by a very long and precisely reproducible incubation period often extending several years without clinical symptoms (10). Once the first clinical symptoms arise, the disease phenotype progresses rapidly (11). The *in vivo* behaviour thus resembles the *in vitro* observations of amyloid fibril growth, with one important distinction: *in vivo*, the fibril mass is continuously diluted as cells divide and degrade misfolded proteins. This behaviour is most pronounced in yeast prions, which divide rapidly. Two yeast prion proteins, Ure2p and Sup35, have been identified, and they share no sequence similarity to PrP. The use of these proteins as model systems for PrP has led to rapid advances in the field of prion diseases.

Exponential growth has been proposed to play an important role in prion diseases (116). If cells divide exponentially, as is certainly the case of yeast prions, the fibril mass has to grow exponentially as well in order to keep up with the dilution effect. A strain failing to do so will inevitably be terminated (11, 23, 116). Tanaka *et al.* (2006) studied physical properties of three different Sup35 prion strains and were able to show that the strain with the strongest phenotype and highest stability, *i.e.*, highest numbers of fibers per cell, surprisingly had the slowest growth rate of the

three. However, this was amply compensated for by a marked increase in fragmentation rate (117). We suggest that some strains may also take advantage of branching as a mechanism to rapidly generate new fibril ends and note that branched fibrils are probably more likely to undergo breakage due to stress than nonbranching fibrils.

6. Specialized techniques

Glucagon fibrillation was studied by a number of biophysical techniques. These include standard techniques (CD, fluorescence spectroscopy, TEM, etc.) as well as more specialized techniques. In this chapter, the specialized techniques are described in more detail in terms of the general layout of the setup as well as the applicability to fibril samples.

6.1 Total internal reflection fluorescence microscopy

TIRFM is based on standard fluorescence microscopy, the main difference being the penetration depth of the excitation light. In TIRFM, only a very thin surface layer is excited by the laser. The setup is sketched in Figure 38.

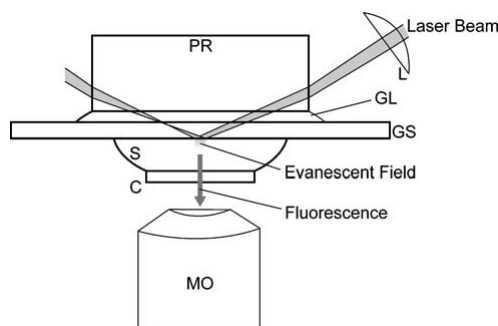


Figure 38. TIRFM setup. A drop of sample solution (S) is placed between a slide glass (GS) and a cover glass (C). A prism (P) lies on top of the glass slide with a thin layer of glycerol (GL) between the two. The laser beam passes through a focusing lens (L) and is incident on the surface of the slide glass at an angle close to the critical angle. In this way, a thin layer of the sample solution is illuminated. The light emitted by fluorescence is collected by the microscope objective (MO). A drop of oil is placed between the cover glass and the objective in order to match the index of refraction. Reprinted from reference (118).

Excitation of a very thin layer close to the surface of the slide glass is achieved through total internal reflection. The principle behind this physical phenomenon is described in the following. A laser beam perpendicular to a glass surface will be almost completely transmitted through the glass. As the angle, θ , between the laser

beam and the glass surface is decreased toward zero degrees, a fraction of the incident light will be reflected. This fraction is in general low compared to the fraction of light transmitted. However, at the critical angle θ_c , a large fraction of the incident light is reflected on behalf of the fraction transmitted. This phenomenon is known as total internal reflection. The exact position of the critical angle depends on the wavelength of the incident light, λ , and the refractive index of the two media, n_1 and n_2 (118).

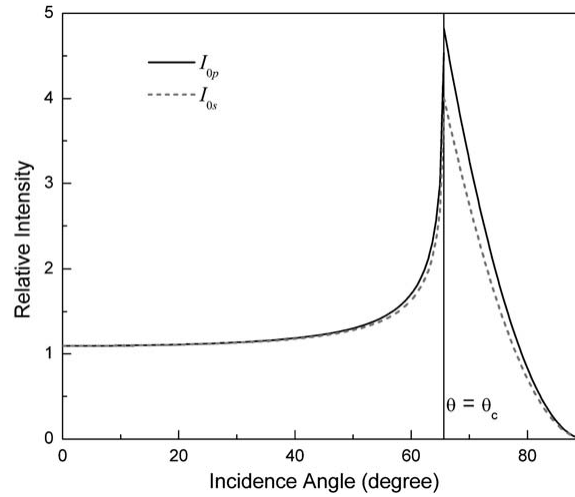


Figure 39. The relative intensity of the evanescent wave as a function of the incident angle, θ . At the critical angle, θ_c , the intensity is several times higher than the intensity of the incoming laser field. In this plot the refractive indices of fused silica ($n_1 = 1.46$) and water ($n_2 = 1.33$) were used together with an Argon wavelength of 532 nm. Reprinted from reference (118)

As it turns out, at the critical angle an evanescent electromagnetic field with the same wavelength as the incident light is generated close to the surface as shown in Figure 39. The intensity of this field is several times higher than the intensity of the incoming laser field and decays exponentially with a penetration depth $d = 1/e$ given by the expression

$$d = \frac{\lambda}{4\pi\sqrt{n_1^2 \sin^2 \theta - n_2^2}}$$

where λ is the wavelength of the incident light in vacuum, and n_1 and n_2 are the refractive indices of the media. In the case where medium 1 is fused silica ($n_1 = 1.46$), medium 2 is water ($n_2 = 1.33$), and the Ar laser has a wavelength of

$\lambda_{Ar} = 455 \text{ nm}$, a penetration depth of 150 nm is obtained (106). Molecules outside this thin volume will not be excited and for this reason the TIRFM technique can be used to study the growth of individual fibrils. The TIRFM technique was first applied to fibril samples by the group of Dr. Goto in 2004 (107).

As fibrillation kinetics very often involve a long lag phase, where only small amounts of fibril mass is formed, preformed seeds are added to the sample solution. The seeds typically bundle together in clusters (107, 108). Radial fibril growth is observed from these clusters by collecting data at fixed time intervals. The technique relies on the fluorescence from a fibril specific dye, in this case ThT. The laser wavelength is chosen so as to match the excitation wavelength of the fluorescent dye.

TIRFM is currently one of just two techniques able to monitor growth of single-fibrils in real-time. The other technique is time-lapse AFM (55). In theory, both techniques are able to visualize secondary nucleation mechanisms (fibril breakage, branching and surface-dependent nucleation). Time-lapse AFM has the great advantage of directly visualizing the organization of the individual protofilaments, allowing for a classification of the individual morphologies and their respective growth rates. However, the interaction with the mica could influence the growth significantly. Goldsbury *et al.* (1999) studied IAPP with time-lapse AFM and were able to show dichotomous branching and measure growth rates (55). They reported, however, that fibrils on the mica consisted of just one protofilament whereas the fibrils from the bulk solution consisted predominantly of higher-order fibrils. The growth rates they reported (approximately 1 nm/min), are very low compared to the growth rates of A β (1-40) (approximately 300 nm/min) and glucagon (approximately 140 nm/min), indicating that mica not only favours simple morphologies but also reduces fibril growth in general. TIRFM, on the other hand, does not give any detailed structural information, but the quartz surface apparently does not affect fibril growth, and is very versatile allowing for a number of different coatings, which enables studying the impact of surfaces on fibril growth (108).

6.2 Fiber diffraction

Fibrils can be aligned along the fibril axis to form fibers. A fiber is hence a macroscopic assembly of fibrils, essentially a one-dimensional crystal, which when exposed to X-rays gives structural information about the molecular organization within the fibril (67). Fibers are often formed by letting a drop of fibrillated sample solution dry between the wax-sealed ends of two end-to-end capillaries (68, 119). If

the molecules are homogeneous and have a regularly repeating motif, the molecules give rise to repeating units aligned in the direction of the fiber axis. However, the repeating units, the unit cells, are likely to have an offset with respect to each other in the direction of the fiber axis, and to be rotationally disordered and averaged across the width of the fiber (120).

In fiber diffraction, symmetry along the fibril axis produces layer lines along the long axis of the fiber. These are the meridional reflections, and include the inter-strand distances of 4.7 Å and, in the case of twisted fibrils, the helical repeat distance. The equatorial reflections, on the other hand, provides information about symmetry in the direction of the fiber diameter, most notably the intersheet distance of approximately 10 Å and the width of the fibrils and protofilaments. Very often, due to the polymorphic nature of fibrils, only the 4.7 and 10 Å reflections on the meridian and equator, respectively, are seen as sharp and distinct peaks. For this reason, fiber diffraction peaks at 4.7 and 10 Å are often used to identify fibrous samples as amyloid fibrils. Fiber diffraction peaks are masked by salt rings, and it is hence necessary to remove buffer salts from the fibril solution before making the fibers (67). The fiber diffraction setup is sketched in Figure 40.

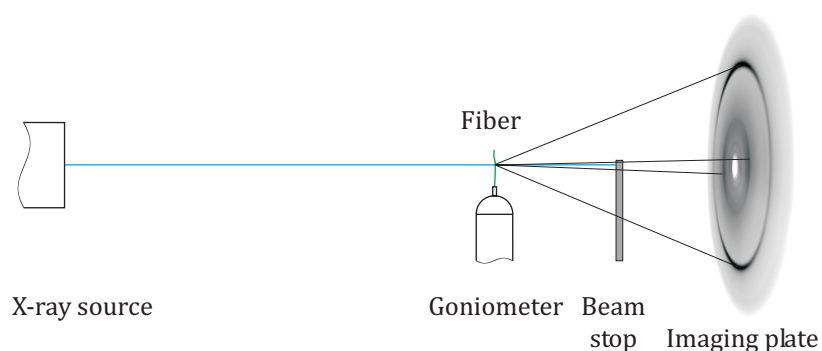


Figure 40. Fiber diffraction setup. An intense X-ray beam from an X-ray source is incident on a fiber aligned in a goniometer. Diffraction peaks are observed on an imaging plate.

If the fibrils are homogeneous and well-aligned within the fiber, it is possible to obtain highly ordered diffraction patterns with many distinct diffraction peaks. In this case it may be possible to make a qualified guess of the space group and unit cell dimensions. This was demonstrated by Makin *et al.* (2005) as described in Section 2.5 (61). However, most often, fiber diffractograms are used to identify fibrils

and to examine if samples formed under different conditions give rise to different morphologies.

6.3 Small-angle light scattering

SALS is a useful technique for studying physical and chemical systems, which are inhomogeneous on length scales of the order of the wavelength of light or larger. Examples of its application include gel formation (121), polymerization processes, and fibrillation (22, 97, 122). In this Ph.D. project, SALS has been applied to study the formation of glucagon and A β (1-40) spherulites. Interestingly, SALS data suggest that glucagon also forms physical gels after the initial spherulite formation through cross-linking of fibrils from neighbouring spherulites (unpublished results). The SALS setup is sketched below.

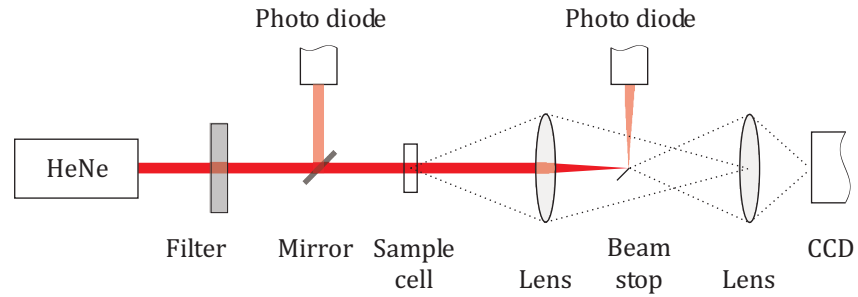


Figure 41. SALS setup. The 632.8 nm HeNe beam passes through an adjustable filter, the sample cell, and a lens before being stopped by the beam stop. Photo diodes before and after the sample cell are used for normalizing the intensity. The first lens on the light path images the scattered light from the sample cell onto the CCD, while the second lens images the beam stop onto the CCD.

The light scattered out of an incoming laser beam is due to the presence of local fluctuations in the dielectric constant of the medium. Letting $\langle \delta\epsilon(\mathbf{r},t)\delta\epsilon(0,t) \rangle$ denote the spatial correlation function of the fluctuations in the dielectric constant at time t and position \mathbf{r} , the intensity distribution of the scattered light is given by (123):

$$I(\mathbf{q}) \propto \int \langle \delta\epsilon(\mathbf{r},t)\delta\epsilon(0,t) \rangle \exp(i\mathbf{q} \cdot \mathbf{r}) d\mathbf{r}$$

where \mathbf{q} is the scattering vector given by the difference between the scattered wave-vector \mathbf{k} and the incident wave-vector \mathbf{k}_0 , $\mathbf{q} = \mathbf{k} - \mathbf{k}_0$. The magnitude of \mathbf{q} is given by:

$$q = \frac{4\pi n}{\lambda} \sin\left(\frac{\theta}{2}\right)$$

where λ is the laser wavelength, n is the index of refraction, and θ is the scattering angle (the angle between \mathbf{k} and \mathbf{k}_0). It can be shown that for small angles, where $\sin(\theta) \approx \theta$, the length scale Λ of the system is given by $\Lambda \approx \lambda / \theta$ (123). The angular ranges accessible on a typical SALS are typically 0.1–10 deg, thus length scales from a few μm up to hundreds of μm can be probed. In contrast to scattering at large angles, the scattering signal at small angles is not directly proportional to the particle mass, as the particle shape is reflected in the form factors at small angles. It is, however, possible to use it as a qualitative measure of particle mass.

7. Conclusion

This thesis has focused on the experimental results elucidating glucagon fibril polymorphism and glucagon fibrillation kinetics. When dissolved in glycine/HCl pH 2.5 buffer, glucagon forms polymorphic fibrils and two of these morphologies—denoted twisted and straight due to their appearance when viewed under an electron microscope—depend strongly on the peptide concentration with twisted fibrils formed at 0.25 mg/mL and straight fibrils formed at 8 mg/mL. The work presented in this thesis show that these two morphologies are most likely due to structural differences at the protofilament level, a phenomenon confirmed in recent years to be a characteristic of prion strains as well.

Intriguingly, the twisted morphology fibrils are unable to sustain growth when cross-seeded at 8 mg/mL glucagon, which normally favors the straight morphology. By studying the self-association of glucagon, it was shown that the inhibition of twisted fibrils—as manifested through a peculiar maximum at 1 mg/mL in the concentration-lag phase plot—correlates with the formation of reversible glucagon trimers. Hence, we conclude that the selection of morphologies arises from the ability of glucagon trimers to specifically inhibit the straight morphology fibrils.

In a set of real-time observations of single-fibril growth on quartz surface layers, glucagon fibrils were monitored for up to 20 hours. The main observation is that glucagon fibrils grow from clusters of seeds into dense spherulitic structures by continuously forming new fibrils by branching. This fibril-dependent formation of new fibril ends is the structural basis for the sigmoid reaction profile first reported for glucagon nearly 40 years ago (124). In TEM of fibrillated samples, we were able to retrieve examples of branching fibrils. Under physiological conditions, seeded solutions of A β (1-40) have been shown to grow solely by addition of monomers (107). We exploited this basic difference in growth mechanisms between A β (1-40) and glucagon to devise a new light scattering method to separate spontaneous nucleation from secondary nucleation. The method is based on seeded reactions: if fibrils grow by addition of monomers to the seed ends alone, fibril mass increases linearly, and increasing the seed concentration increases the slope of fibril mass formation. If, on the other hand, fibrils formed from seeds are also capable of forming new fibrils by a secondary mechanism, increasing the seed concentration will decrease the lag phase.

Consensus in the field for the past 50 years has established that fibrils are non-branched structures (3), and most structural studies have since then confirmed this

view. As the sigmoid reaction profile—a hallmark of secondary processes—is common to studies of fibril kinetics, we would not be surprised if branching turns out to be a widespread feature of amyloid fibril formation.

The thesis also highlights the parallelism of glucagon fibrillation with findings in prion diseases, and hence demonstrates the reason why peptides not directly related to amyloid diseases are conveniently used as model systems of fibrillation.

8. Papers

8.1 Glucagon amyloid-like fibril morphology is selected via morphology-dependent growth inhibition

8.2 Branching in amyloid fibril growth

9. References

1. Dobson, C. M. (1999) Protein misfolding, evolution and disease *Trends in Biochemical Sciences* **24**, 329-332.
2. Kyle, R. A. (2001) Amyloidosis: A convoluted story *British Journal of Haematology* **114**, 529-538.
3. Cohen, A. S. & Calkins, E. (1959) Electron Microscopic Observations on A Fibrous Component in Amyloid of Diverse Origins *Nature* **183**, 1202-1203.
4. Otzen, D. & Nielsen, P. (2008) We find them here, we find them there: Functional bacterial amyloid *Cellular and Molecular Life Sciences (CMLS)* (Published online ahead of print).
5. Claverie, J. M. (2005) Fewer Genes, More Noncoding RNA *Science* **309**, 1529-1530.
6. Thomas, P. J., Qu, B. H., & Pedersen, P. L. (1995) Defective Protein-Folding As A Basis of Human-Disease *Trends in Biochemical Sciences* **20**, 456-459.
7. Uversky, V. N. & Fink, A. L. (2004) Conformational constraints for amyloid fibrillation: the importance of being unfolded *Biochimica et Biophysica Acta-Proteins and Proteomics* **1698**, 131-153.
8. Monsellier, E. & Chiti, F. (2007) Prevention of amyloid-like aggregation as a driving force of protein evolution *Embo Reports* **8**, 737-742.
9. Dobson, C. M. (2002) Protein-misfolding diseases: Getting out of shape *Nature* **418**, 729-730.
10. Lansbury, P. T. & Lashuel, H. A. (2006) A century-old debate on protein aggregation and neurodegeneration enters the clinic *Nature* **443**, 774-779.
11. Collinge, J. & Clarke, A. R. (2007) A general model of prion strains and their pathogenicity *Science* **318**, 930-936.
12. Drucker, D. J. (2005) Biologic actions and therapeutic potential of the proglucagon-derived peptides *Nature Clinical Practice Endocrinology & Metabolism* **1**, 22-31.
13. Miki, T., Liss, B., Minami, K., Shiuchi, T., Saraya, A., Kashima, Y., Horiuchi, M., Ashcroft, F., Minokoshi, Y., Roeper, J. *et al.* (2001) ATP-sensitive K⁺ channels in the hypothalamus are essential for the maintenance of glucose homeostasis *Nat Neurosci* **4**, 507-512.
14. Drucker, D. J. (1998) Glucagon-like peptides *Diabetes* **47**, 159-169.
15. Jang, H. J., Kokrashvili, Z., Theodorakis, M. J., Carlson, O. D., Kim, B. J., Zhou, J., Kim, H. H., Xu, X., Chan, S. L., Juhaszova, M. *et al.* (2007) Gut-expressed gustducin and taste receptors regulate secretion of glucagon-like peptide-1 *Proceedings of the National Academy of Sciences of the United States of America* **104**, 15069-15074.

16. Christensen, S., Moeller, E. H., Bonde, C., & Lilleoere, A. M. (2007) Preliminary studies of the physical stability of a glucagon-like peptide-1 derivate in the presence of metal ions *European Journal of Pharmaceutics and Biopharmaceutics* **66**, 366-371.
17. Pedersen, J. S., Dikov, D., Flink, J. L., Hjuler, H. A., Christiansen, G., & Otzen, D. E. (2006) The changing face of glucagon fibrillation: Structural polymorphism and conformational imprinting *J. Mol. Biol.* **355**, 501-523.
18. Kodali, R. & Wetzel, R. (2007) Polymorphism in the intermediates and products of amyloid assembly *Current Opinion in Structural Biology* **17**, 48-57.
19. Andersen, C. B., Otzen, D., Christiansen, G., & Rischel, C. (2007) Glucagon Amyloid-like Fibril Morphology Is Selected via Morphology-Dependent Growth Inhibition *Biochemistry* **46**, 7314-7324.
20. Padrick, S. B. & Miranker, A. D. (2002) Islet amyloid: Phase partitioning and secondary nucleation are central to the mechanism of fibrillogenesis *Biochemistry* **41**, 4694-4703.
21. Pedersen, J. S., Flink, J. M., Dikov, D., & Otzen, D. E. (2006) Sulfates dramatically stabilize a salt-dependent type of glucagon fibrils *Biophys. J.* **90**, 4181-4194.
22. Manno, M., Craparo, E. F., Martorana, V., Bulone, D., & San Biagio, P. L. (2006) Kinetics of insulin aggregation: Disentanglement of amyloid fibrillation from large-size cluster formation *Biophys. J.* **90**, 4585-4591.
23. Collins, S. R., Douglass, A., Vale, R. D., & Weissman, J. S. (2004) Mechanism of prion propagation: Amyloid growth occurs by monomer addition *Plos Biology* **2**, 1582-1590.
24. Crick, F. (1970) Central Dogma of Molecular Biology *Nature* **227**, 561-563.
25. Anfinsen, C. B., Haber, E., Sela, M., & White, F. H. (1961) Kinetics of Formation of Native Ribonuclease During Oxidation of Reduced Polypeptide Chain *Proceedings of the National Academy of Sciences of the United States of America* **47**, 1309-1314.
26. Levinthal, C. (1968) Are There Pathways for Protein Folding *Journal de Chimie Physique et de Physico-Chimie Biologique* **65**, 44-45.
27. Dobson, C. M. (2003) Protein folding and misfolding *Nature* **426**, 884-890.
28. Dill, K. A. & Chan, H. S. (1997) From Levinthal to pathways to funnels *Nature Structural Biology* **4**, 10-19.
29. Fersht A. (1999) *Structure and mechanism in protein science* (Freeman, New York).
30. Dobson, C. M. (2004) Principles of protein folding, misfolding and aggregation *Seminars in Cell & Developmental Biology* **15**, 3-16.
31. Chiti, F., Webster, P., Taddei, N., Clark, A., Stefani, M., Ramponi, G., & Dobson, C. M. (1999) Designing conditions for in vitro formation of amyloid protofilaments and

fibrils *Proceedings of the National Academy of Sciences of the United States of America* **96**, 3590-3594.

32. Roher, A. E., Lowenson, J. D., Clarke, S., Wolkow, C., Wang, R., Cotter, R. J., Reardon, I. M., Zurcherneely, H. A., Heinrichson, R. L., Ball, M. J. *et al.* (1993) Structural Alterations in the Peptide Backbone of Beta-Amyloid Core Protein May Account for Its Deposition and Stability in Alzheimers-Disease *Journal of Biological Chemistry* **268**, 3072-3083.
33. Pawar, A. P., Dubay, K. F., Zurdo, J., Chiti, F., Vendruscolo, M., & Dobson, C. M. (2005) Prediction of "aggregation-prone" and "aggregation-susceptible" regions in proteins associated with neurodegenerative diseases *Journal of Molecular Biology* **350**, 379-392.
34. Steward, A., Adhya, S., & Clarke, J. (2002) Sequence conservation in Ig-like domains: The role of highly conserved proline residues in the fibronectin type III superfamily *Journal of Molecular Biology* **318**, 935-940.
35. Pedersen, J. S., Christensen, G., & Otzen, D. E. (2004) Modulation of S6 fibrillation by unfolding rates and gatekeeper residues *Journal of Molecular Biology* **341**, 575-588.
36. Parrini, C., Taddei, N., Ramazzotti, M., Degl'Innocenti, D., Ramponi, G., Dobson, C. M., & Chiti, F. (2005) Glycine residues appear to be evolutionarily conserved for their ability to inhibit aggregation *Structure* **13**, 1143-1151.
37. Lighthouse Data (2006).
38. Schade, D. S. & Eaton, R. P. (1975) Glucagon Regulation of Plasma Ketone-Body Concentration in Human Diabetes *Journal of Clinical Investigation* **56**, 1340-1344.
39. Drucker, D. J. (1998) Glucagon-like peptides *Diabetes* **47**, 159-169.
40. Drucker, D. J. (2005) Biologic actions and therapeutic potential of the proglucagon-derived peptides *Nature Clinical Practice Endocrinology & Metabolism* **1**, 22-31.
41. Fernandez-Escamilla, A. M., Rousseau, F., Schymkowitz, J., & Serrano, L. (2004) Prediction of sequence-dependent and mutational effects on the aggregation of peptides and proteins *Nature Biotechnology* **22**, 1302-1306.
42. Trovato, A., Chiti, F., Maritan, A., & Seno, F. (2006) Insight into the structure of amyloid fibrils from the analysis of globular proteins *Plos Computational Biology* **2**, 1608-1618.
43. Pedersen, J. S., Dikov, D., & Otzen, D. E. (2006) N- and C-terminal hydrophobic patches are involved in fibrillation of glucagon *Biochemistry* **45**, 14503-14512.
44. Serrano, L., Schymkowitz, J., and Rousseau, F. (5-11-2007) Tango - A computer algorithm for prediction of aggregating regions in unfolded polypeptide chains <http://tango.crg.es/>.
45. Trovato, A., Maritan, A., & Seno, F. (2007) Aggregation of natively folded proteins: a theoretical approach *Journal of Physics-Condensed Matter* **19**.

46. Kheterpal, I., Chen, M., Cook, K. D., & Wetzel, R. (2006) Structural differences in A beta amyloid protofibrils and fibrils mapped by hydrogen exchange - Mass spectrometry with on-line proteolytic fragmentation *Journal of Molecular Biology* **361**, 785-795.
47. Frare, E., Mossuto, M. F., de Laureto, P. P., Dumoulin, M., Dobson, C. M., & Fontana, A. (2006) Identification of the core structure of lysozyme amyloid fibrils by proteolysis *Journal of Molecular Biology* **361**, 551-561.
48. Myers, S. L., Thomson, N. H., Radford, S. E., & Ashcroft, A. E. (2006) Investigating the structural properties of amyloid-like fibrils formed in vitro from beta 2-microglobulin using limited proteolysis and electrospray ionisation mass spectrometry *Rapid Communications in Mass Spectrometry* **20**, 1628-1636.
49. Stromer, T. & Serpell, L. C. (2005) Structure and morphology of the Alzheimer's amyloid fibril *Microscopy Research and Technique* **67**, 210-217.
50. Fandrich, M. & Dobson, C. M. (2002) The behaviour of polyamino acids reveals an inverse side chain effect in amyloid structure formation *Embo Journal* **21**, 5682-5690.
51. Krishnan, R. & Lindquist, S. L. (2005) Structural insights into a yeast prion illuminate nucleation and strain diversity *Nature* **435**, 765-772.
52. Anderson, M., Bocharova, O. V., Makarava, N., Breydo, L., Salnikov, V. V., & Baskakov, I. V. (2006) Polymorphism and ultrastructural organization of prion protein amyloid fibrils: An insight from high resolution atomic force microscopy *J. Mol. Biol.* **358**, 580-596.
53. Kad, N. M., Myers, S. L., Smith, D. P., Smith, D. A., Radford, S. E., & Thomson, N. H. (2003) Hierarchical assembly of beta(2)-microglobulin amyloid in vitro revealed by atomic force microscopy *J. Mol. Biol.* **330**, 785-797.
54. Dong, M., Hovgaard, M. B., Xu, S., Otzen, D., & Besenbacher, F. (2006) AFM Study of glucagon fibrillation via oligomeric structures resulting in interwoven fibrils *Nanotech.* **17**, 4003-4009.
55. Goldsbury, C., Kistler, J., Aebi, U., Arvinte, T., & Cooper, G. J. S. (1999) Watching amyloid fibrils grow by time-lapse atomic force microscopy *J. Mol. Biol.* **285**, 33-39.
56. Goldsbury, C. S., Wirtz, S., Muller, S. A., Sunderji, S., Wicki, P., Aebi, U., & Frey, P. (2000) Studies on the in vitro assembly of A beta 1-40: Implications for the search for A beta fibril formation inhibitors *J. Struct. Biol.* **130**, 217-231.
57. De Jong, K. L., Incedon, B., Yip, C. M., & DeFelippis, M. R. (2006) Amyloid fibrils of glucagon characterized by high-resolution atomic force microscopy *Biophys. J.* **91**, 1905-1914.
58. Jimenez, J. L., Nettleton, E. J., Bouchard, M., Robinson, C. V., Dobson, C. M., & Saibil, H. R. (2002) The protofilament structure of insulin amyloid fibrils *Proceedings of the National Academy of Sciences of the United States of America* **99**, 9196-9201.

59. Tycko, R. (2003) Insights into the amyloid folding problem from solid-state NMR *Biochemistry* **42**, 3151-3159.
60. Kheterpal, I., Williams, A., Murphy, C., Bledsoe, B., & Wetzel, R. (2001) Structural features of the A beta amyloid fibril elucidated by limited proteolysis *Biochemistry* **40**, 11757-11767.
61. Makin, O. S., Atkins, E., Sikorski, P., Johansson, J., & Serpell, L. C. (2005) Molecular basis for amyloid fibril formation and stability *Proceedings of the National Academy of Sciences of the United States of America* **102**, 315-320.
62. Nelson, R., Sawaya, M. R., Balbirnie, M., Madsen, A. O., Riek, C., Grothe, R., & Eisenberg, D. (2005) Structure of the cross-beta spine of amyloid-like fibrils *Nature* **435**, 773-778.
63. Sawaya, M. R., Sambashivan, S., Nelson, R., Ivanova, M. I., Sievers, S. A., Apostol, M. I., Thompson, M. J., Balbirnie, M., Wiltzius, J. J. W., McFarlane, H. T. *et al.* (2007) Atomic structures of amyloid cross-beta spines reveal varied steric zippers *Nature* **447**, 453-457.
64. Knowles, T. P. J., Smith, J. F., Craig, A., Dobson, C. M., & Welland, M. E. (2006) Spatial persistence of angular correlations in amyloid fibrils *Phys. Rev. Lett.* **96**, 238301.
65. Glenner, G. G., Eanes, E. D., Bladen, H. A., Linke, R. P., & Termine, J. D. (1974) Beta-Pleated Sheet Fibrils - Comparison of Native Amyloid with Synthetic Protein Fibrils *J. Histochem. & Cytochem.* **22**, 1141-1158.
66. Sunde, M. & Blake, C. (1997) The structure of amyloid fibrils by electron microscopy and X-ray diffraction in *Advances in protein chemistry* pp. 123-159.
67. Serpell, L. C., Fraser, P. E., & Sunde, M. (1999) X-Ray fiber diffraction of amyloid fibrils in *Methods in Enzymology*, ed. Ronald, W. (Academic Press, New York), pp. 526-536.
68. Holm, N. K., Jespersen, S. K., Thomassen, L. V., Wolff, T. Y., Sehgal, P., Thomsen, L. A., Christiansen, G., Andersen, C. B., Knudsen, A. D., & Otzen, D. E. (2007) Aggregation and fibrillation of bovine serum albumin *Biochimica et Biophysica Acta-Proteins and Proteomics* **1774**, 1128-1138.
69. Makin, O. S. & Serpell, L. C. (2005) Structures for amyloid fibrils *Febs Journal* **272**, 5950-5961.
70. Sumner Makin, O. & Serpell, L. C. (2004) Structural Characterisation of Islet Amyloid Polypeptide Fibrils *Journal of Molecular Biology* **335**, 1279-1288.
71. Makin, O. S., Sikorski, P., & Serpell, L. C. (2007) CLEARER: a new tool for the analysis of X-ray fibre diffraction patterns and diffraction simulation from atomic structural models *Journal of Applied Crystallography* **40**, 966-972.
72. Khurana, R., Coleman, C., Ionescu-Zanetti, C., Carter, S. A., Krishna, V., Grover, R. K., Roy, R., & Singh, S. (2005) Mechanism of thioflavin T binding to amyloid fibrils *Journal of Structural Biology* **151**, 229-238.

73. Khurana, R., Uversky, V. N., Nielsen, L., & Fink, A. L. (2001) Is Congo red an amyloid-specific dye? *Journal of Biological Chemistry* **276**, 22715-22721.
74. Groenning, M., Norrman, M., Flink, J. M., van de Weert, M., Bukrinsky, J. T., Schluckebier, G., & Frokjaer, S. (2007) Binding mode of Thioflavin T in insulin amyloid fibrils *Journal of Structural Biology* **159**, 483-497.
75. Chen, Y. & Barkley, M. D. (1998) Toward Understanding Tryptophan Fluorescence in Proteins *Biochemistry* **37**, 9976-9982.
76. Kihara, M., Chatani, E., Iwata, K., Yamamoto, K., Matsuura, T., Nakagawa, A., Naiki, H., & Goto, Y. (2006) Conformation of Amyloid Fibrils of beta2-Microglobulin Probed by Tryptophan Mutagenesis *Journal of Biological Chemistry* **281**, 31061-31069.
77. Yang, J. T., Wu, C. S., & Martinez, H. M. (1986) [11] Calculation of protein conformation from circular dichroism in *Methods in Enzymology Enzyme Structure Part K*, ed. Hirs and Serge, H. W. (Academic Press, pp. 208-269.
78. Dafforn, T. R. & Rodger, A. (2004) Linear dichroism of biomolecules: which way is up? *Current Opinion in Structural Biology* **14**, 541-546.
79. Dafforn, T. R., Rajendra, J., Halsall, D. J., Serpell, L. C., & Rodger, A. (2004) Protein fiber linear dichroism for structure determination and kinetics in a low-volume, low-wavelength couette flow cell *Biophys. J.* **86**, 404-410.
80. Adachi, R., Yamaguchi, K., Yagi, H., Sakurai, K., Naiki, H., & Goto, Y. (2007) Flow-induced alignment of amyloid protofilaments revealed by linear dichroism *Journal of Biological Chemistry* **282**, 8978-8983.
81. Yagi, H., Kusaka, E., Hongo, K., Mizobata, T., & Kawata, Y. (2005) Amyloid fibril formation of alpha-synuclein is accelerated by preformed amyloid seeds of other proteins: implications for the mechanism of transmissible conformational diseases *J. Biol. Chem.* **280**, 38609-38616.
82. O'Nuallain, B., Williams, A. D., Westermarck, P., & Wetzel, R. (2004) Seeding specificity in amyloid growth induced by heterologous fibrils *J. Biol. Chem.* **279**, 17490-17499.
83. Lindner, H. & Glatter, O. (2000) Determination of absolute intensity and molecular weight of small colloidal particles in the presence of some large aggregates. A combined study using static and dynamic light scattering *Particle & Particle Systems Characterization* **17**, 89-95.
84. Oberer, M., Lindner, H., Glatter, O., Kratky, C., & Keller, W. (1999) Thermodynamic properties and DNA binding of the ParD protein from the broad host-range plasmid RK2/RP4 killing system *Biological Chemistry* **380**, 1413-1420.
85. Blundell, T. L. (1983) The Conformation of Glucagon in *Handbook of Experimental Pharmacology*, ed. Lefebvre, P. (Springer-Verlag, Berlin), pp. 37-56.
86. Wagman, M. E., Dobson, C. M., & Karplus, M. (1980) Proton Nmr-Studies of the Association and Folding of Glucagon in Solution *Febs Letters* **119**, 265-270.

87. Sasaki, K., Dockerill, S., Adamiak, D. A., Tickle, I. J., & Blundell, T. (1975) X-Ray Analysis of Glucagon and Its Relationship to Receptor-Binding *Nature* **257**, 751-757.
88. Hong, D. P. & Fink, A. L. (2005) Independent heterologous fibrillation of insulin and its B-chain peptide *Biochemistry* **44**, 16701-16709.
89. Devlin, G. L., Knowles, T. P. J., Squires, A., McCammon, M. G., Gras, S. L., Nilsson, M. R., Robinson, C. V., Dobson, C. M., & MacPhee, C. E. (2006) The component polypeptide chains of bovine insulin nucleate or inhibit aggregation of the parent protein in a conformation-dependent manner *Journal of Molecular Biology* **360**, 497-509.
90. Conway, K. A., Lee, S. J., Rochet, J. C., Ding, T. T., Williamson, R. E., & Lansbury, P. T. (2000) Acceleration of oligomerization, not fibrillization, is a shared property of both alpha-synuclein mutations linked to early-onset Parkinson's disease: Implications for pathogenesis and therapy *Proceedings of the National Academy of Sciences of the United States of America* **97**, 571-576.
91. Harper, J. D., Wong, S. S., Lieber, C. M., & Lansbury, P. T. (1999) Assembly of A beta amyloid protofibrils: An in vitro model for a possible early event in Alzheimer's disease *Biochemistry* **38**, 8972-8980.
92. Nielsen, L., Khurana, R., Coats, A., Frokjaer, S., Brange, J., Vyas, S., Uversky, V. N., & Fink, A. L. (2001) Effect of environmental factors on the kinetics of insulin fibril formation: Elucidation of the molecular mechanism *Biochem.* **40**, 6036-6046.
93. Librizzi, F. & Rischel, C. (2005) The kinetic behavior of insulin fibrillation is determined by heterogeneous nucleation pathways *Protein Sci* **14**, 3129-3134.
94. Ferrone, F. (1999) Analysis of protein aggregation kinetics in *Meth. Enzym.* pp. 256-274.
95. Kumar, S., Mohanty, S. K., & Udgaonkar, J. B. (2007) Mechanism of formation of amyloid protofibrils of barstar from soluble oligomers: Evidence for multiple steps and lateral association coupled to conformational conversion *Journal of Molecular Biology* **367**, 1186-1204.
96. Gosal, W. S., Morten, I. J., Hewitt, E. W., Smith, D. A., Thomson, N. H., & Radford, S. E. (2005) Competing pathways determine fibril morphology in the self-assembly of beta(2)-microglobulin into amyloid *Journal of Molecular Biology* **351**, 850-864.
97. Carrotta, R., Manno, M., Bulone, D., Martorana, V., & San Biagio, P. L. (2005) Protofibril formation of amyloid beta-protein at low pH via a non-cooperative elongation mechanism *J. Biol. Chem.* **280**, 30001-30008.
98. Smith, A. M., Jahn, T. R., Ashcroft, A. E., & Radford, S. E. (2006) Direct observation of oligomeric species formed in the early stages of amyloid fibril formation using electrospray ionisation mass spectrometry *J. Mol. Biol.* **364**, 9-19.
99. Vestergaard, B., Groenning, M., Roessle, M., Kastrup, J. S., van de Weert, M., Flink, J. M., Frokjaer, S., Gajhede, M., & Svergun, D. I. (2007) A helical structural nucleus is the primary elongating unit of insulin amyloid fibrils *Plos Biology* **5**, 1089-1097.

100. Hamill, A. C., Wang, S. C., & Lee, C. T. (2007) Solution Structure of an Amyloid-Forming Protein During Photoinitiated Hexamer-Dodecamer Transitions Revealed through Small-Angle Neutron Scattering *Biochemistry* **46**, 7694-7705.
101. Silveira, J. R., Raymond, G. J., Hughson, A. G., Race, R. E., Sim, V. L., Hayes, S. F., & Caughey, B. (2005) The most infectious prion protein particles *Nature* **437**, 257-261.
102. Flyvbjerg, H., Jobs, E., & Leibler, S. (1996) Kinetics of self-assembling microtubules: An "inverse problem" in biochemistry *Proc. Natl. Acad. Sci.* **93**, 5975-5979.
103. Librizzi, F. & Rischel, C. (2005) The kinetic behavior of insulin fibrillation is determined by heterogeneous nucleation pathways *Protein Sci* **14**, 3129-3134.
104. Ruschak, A. M. & Miranker, A. D. (2007) Fiber-dependent amyloid formation as catalysis of an existing reaction pathway *Proc. Natl. Acad. Sci.* **104**, 12341-12346.
105. Smith, J. F., Knowles, T. P. J., Dobson, C. M., MacPhee, C. E., & Welland, M. E. (2006) Characterization of the nanoscale properties of individual amyloid fibrils *Proc. Natl. Acad. Sci.* **103**, 15806-15811.
106. Ban, T. & Goto, Y. (2006) Direct observation of amyloid growth monitored by total internal reflection fluorescence microscopy in *Meth. Enzym.* pp. 91-102.
107. Ban, T., Hoshino, M., Takahashi, S., Hamada, D., Hasegawa, K., Naiki, H., & Goto, Y. (2004) Direct observation of Abeta amyloid fibril growth and inhibition *J. Mol. Biol.* **344**, 757-767.
108. Ban, T., Morigaki, K., Yagi, H., Kawasaki, T., Kobayashi, A., Yuba, S., Naiki, H., & Goto, Y. (2006) Real-time and single fibril observation of the formation of amyloid beta spherulitic structures *J. Biol. Chem.* **281**, 33677-33683.
109. Ban, T., Hamada, D., Hasegawa, K., Naiki, H., & Goto, Y. (2003) Direct observation of amyloid fibril growth monitored by thioflavin T fluorescence *Journal of Biological Chemistry* **278**, 16462-16465.
110. Rogers, S. S., Krebs, M. R. H., Bromley, E. H. C., van der Linden, E., & Donald, A. M. (2006) Optical microscopy of growing insulin amyloid spherulites on surfaces in vitro *Biophys. J.* **90**, 1043-1054.
111. Blackley, H. K. L., Sanders, G. H. W., Davies, M. C., Roberts, C. J., Tendler, S. J. B., & Wilkinson, M. J. (2000) In-situ atomic force microscopy study of beta-amyloid fibrilization *Journal of Molecular Biology* **298**, 833-840.
112. Jackson, G. S. & Collinge, J. (2001) The molecular pathology of CJD: old and new variants *Journal of Clinical Pathology-Molecular Pathology* **54**, 393-399.
113. Fraser, H. & Dickinso, A. G. (1973) Scrapie in Mice - Agent-Strain Differences in Distribution and Intensity of Grey Matter Vacuolation *Journal of Comparative Pathology* **83**, 29-40.
114. Collinge, J., Sidle, K. C. L., Meads, J., Ironside, J., & Hill, A. F. (1996) Molecular analysis of prion strain variation and the aetiology of 'new variant' CJD *Nature* **383**, 685-690.

115. Hill, A. F., Desbruslais, M., Joiner, S., Sidle, K. C. L., Gowland, I., Collinge, J., Doey, L. J., & Lantos, P. (1997) The same prion strain causes vCJD and BSE *Nature* **389**, 448-450.
116. Masel, J., Jansen, V. A. A., & Nowak, M. A. (1999) Quantifying the kinetic parameters of prion replication *Biophys. Chem.* **77**, 139-152.
117. Tanaka, M., Collins, S. R., Toyama, B. H., & Weissman, J. S. (2006) The physical basis of how prion conformations determine strain phenotypes *Nature* **442**, 585-589.
118. Wazawa, T. & Ueda, M. (2005) *Total internal reflection fluorescence microscopy in single molecule nanobioscience* (Springer-Verlag, Berlin Heidelberg).
119. Makin, O. S., Sikorski, P., & Serpell, L. C. (2006) Diffraction to study protein and peptide assemblies *Current Opinion in Chemical Biology* **10**, 417-422.
120. Kensal E. van Holde, W. Curtis Johnson, & P. Shing Ho (1998) *Principles of Physical Biochemistry* (Prentice-Hall, Inc., Upper Saddle River, New Jersey 07458).
121. Bulone, D., Giacomazza, D., Martorana, V., Newman, J., & San Biagio, P. L. (2004) Ordering of agarose near the macroscopic gelation point *Phys. Rev. E* **69**, 041401.
122. Carrotta, R., Barthes, J., Longo, A., Martorana, V., Manno, M., Portale, G., & Biagio, P. L. S. (2007) Large size fibrillar bundles of the Alzheimer amyloid beta-protein *Euro. Biophys. J. with Biophys. Let.* **36**, 701-709.
123. Ferri, F. (1997) Use of a charge coupled device camera for low-angle elastic light scattering *Review of Scientific Instruments* **68**, 2265-2274.
124. Beaven, G. H., Gratzer, W. B., & Davies, H. G. (1969) Formation and Structure of Gels and Fibrils from Glucagon *Euro. Jour. Biochem.* **11**, 37-42.